Simulation Study of Aspects of the Classical Hydrogen Atom Interacting with Electromagnetic Radiation: Elliptical Orbits

Daniel C. Cole and Yi Zou

Dept. of Manufacturing Engineering, 15 St. Mary's Street,

Boston University, Brookline, Massachusetts 02446

Key words: hydrogen, Rydberg, stochastic, electrodynamics, simulation classical, nonlinear

Abstract

The present study examines the behavior of a classical charged point particle in near-elliptic orbits about an infinitely massive and oppositely charged nucleus, while acted upon by applied electromagnetic radiation. As recently shown for near-circular orbits, and now extended here to the elliptical case, rather surprising nonlinear dynamical effects are readily produced for this simple system. A broad range of stability-like conditions can be achieved by applying radiation to this classical atom. A perfect balance condition is examined, which requires an infinite number of plane waves representing harmonics of the orbital motion. By applying a scale factor to this radiation, stability-like conditions are produced where periodic variations in semimajor and semiminor axes occur for extended periods of time, before orbital decay eventually takes over due to the effects of radiation reaction. This work is expected to lead to both practical suggestions on experimental ideas involving controlling ionization and stabilization conditions, as well as hopefully aiding in theoretical explorations of stochastic electrodynamics.

I. INTRODUCTION

The research described in the present article is a natural continuation of research reported in Ref. [1]. There, the behavior of a classical model of the hydrogen atom was examined consisting of a classical charged particle representing an electron, with charge $-e$ and mass m, orbited an infinitely massive nucleus, with charge $+e$. The specific situation was examined where only near-circular orbits were considered, with classical radiation reaction taken into account. Circularly polarized (CP) plane waves acted upon the system, with the direction of the CP waves traveling along the direction perpendicular to the orbit of the classical electron.

Probably most readers' initial reaction would be to question, both physically and mathematically, the interest in such an apparently archaic and limited physical system. At first glance, clearly it does not correspond to what is observed in nature. With no radiation or other forces acting, except the effect of radiation reaction due to the natural accelerated motion of the classical electron as it orbits the classical nucleus, the electron's orbit continually spirals inward. The result is the collapse of the orbit, which was discussed extensively by physicists in the early 1900s, and which Bohr's early quantized model first attempted to rectify. Moreover, the restriction to circular orbits in Ref. [1] might make one suspect that besides being of limited physical interest, there seems little of mathematical interest as well.

However, as discussed in Sec. I of Ref. [1], there are at least three reasons why this system is physically of interest and worth investigating. Moreover, as shown throughout the remainder of Ref. [1], this simple circular system has a surprising number of fascinating nonlinear behaviors that apparently have not been noticed nor studied by previous researchers.

In quick summary, three physical reasons for probing on this system are: (1) such a system is the first-order description for excited Rydberg atoms in high energy states, which have received considerable attention both theoretically and experimentally in recent years [2],[3],[4],[5],[6],[7]; (2) new applications may be possible by studying this simplest of atomic systems, with applied radiation, ranging from ionization considerations for use in ion implantation and plasma etching, to the study of controlling simple chemical reactions [8],[9],[10],[11],[12]; and (3) this system, when considered in conjunction with classical electromagnetic zero-point radiation, may well aid in understanding better what is either

lacking, and/or appropriate, in the classical electromagnetic theory of nature often called stochastic electrodynamics (SED) [13],[14],[15],[16].

Moreover, another reason why this system is not so outlandish to study is the following, as quoted from Ref. [17]: "Classical and semiclassical methods are unrivaled in providing an intuitive and computationally tractable approach to the study of atomic, molecular, and nuclear dynamics. An important advantage of such methods is their ability to uncover in a single picture underlying structures that may be hard to extract from the profusion of data supplied by detailed quantum calculations."

As for the interesting nonlinear results demonstrated in Ref. [1], near-circular orbits were studied for a classical charged particle described by the classical Lorentz-Dirac equation, where the speed of the charged particle was much less than that of the speed of light, so that a nonrelativistic approximation could be safely made. By sending a CP plane wave, normal to the plane of the orbit, as shown in Fig. 1, with a frequency precisely equal to the circular orbit, then the amplitude of the electric field can be chosen to precisely balance the classical radiation reaction, thereby resulting in a perfectly circular orbit. Such a situation is probably not too surprising, although it is clearly a very hypothetical situation requiring perfect balance. However, what was shown to be surprising, is that beside this very precise balance point, there is a large range of stability-like conditions that exist for amplitudes of the electric field greater than this balance point. For larger amplitudes, the radius undergoes a gradual increase, as it spirals out due to the increased force, then it spirals back in, due to the Lorentz force from the plane wave becoming out of phase with the velocity of the orbiting particle. This pattern continues over and over, with eventual decay sharply setting in at a clear transition point, when the phases can no longer be properly matched. As shown in Figs. (3a) and (4) in Ref. [1], the larger the amplitude of the applied electric field, the faster this behavior repeats itself and the larger the deviation becomes for the radius from the initial radius. To our knowledge, this behavior has not been investigated nor reported elsewhere.

In the present article, this study will now be carried over to more general orbits, namely, near elliptic ones. We will again restrict our attention to nonrelativistic conditions, as we intend to report on relativistic conditions in separate, future work. In Sec. II, the equations of motion and a quick summary of unperturbed Keplerian (elliptical) motion are provided. Section III turns to the situation where first only radiation reaction acts for the orbiting

classical electron in an initial elliptical orbit. Finding the right set of applied radiation conditions to balance the radiation reaction is clearly more complicated than in the circular case. Instead of a single set of plane waves with a single frequency matching the orbit, now an infinite number of plane waves, with each being an increasing harmonic of this frequency, are required to establish perfect balance. As with the circular case, perhaps this result is not too surprising, although the spectrum necessary to accomplish this task certainly strikes us as intriguing. However, as shown in Sec. IV, where the numerical results are explored for different elliptical and applied radiation conditions, one can see that even when perfect balance is not established, there is a very large range of stability-like conditions that exist, particularly for radiation of larger scaled amplitudes than that required for perfect balance. The results correspond nicely with the circular case, with spiraling motion occurring in and out for long periods of time before decay eventually sets in.

Section V contains some concluding remarks and plans for future explorations.

II. EQUATIONS OF MOTION AND ELLIPTICAL SUMMARY

The starting point of the present study is again making nonrelativistic approximations to the Lorentz-Dirac equation, as discussed in Ref. [1]. The numerical solution is again implemented by treating it as six first-order differential equations, with

$$\dot{\mathsf{z}} = \frac{\mathsf{p}}{m} \quad , \tag{1}$$

and

$$\dot{\mathsf{p}} = -\frac{e^2 \mathsf{z}}{|\mathsf{z}|^3} + \mathsf{R}_{\rm reac} + (-e)\left\{\mathsf{E}\left[\mathsf{z}\left(t\right), t\right] + \frac{\dot{\mathsf{z}}}{c} \times \mathsf{B}\left[\mathsf{z}\left(t\right), t\right]\right\} \quad , \tag{2}$$

where the right sides of the above two equations are expressed in terms of $\mathsf{z}\left(t\right)$ and $\mathsf{p}\left(t\right)$, the applied radiation electric and magnetic fields are given by E and B, and where the radiation reaction term of $\mathsf{R}_{\rm reac}$ is approximated by

$$\mathsf{R}_{\rm reac} \approx \frac{2}{3}\frac{e^2}{c^3}\frac{d^3\mathsf{z}}{dt^3} \approx \frac{2}{3}\frac{e^2}{c^3}\frac{d}{dt}\left[\frac{1}{m}\left(-\frac{e^2\mathsf{z}}{|\mathsf{z}|^3} - e\left\{\mathsf{E}\left[\mathsf{z}\left(t\right), t\right] + \frac{\dot{\mathsf{z}}}{c} \times \mathsf{B}\left[\mathsf{z}\left(t\right), t\right]\right\}\right)\right] \quad . \tag{3}$$

Using Cartesian coordinates, with $u_1 = z_1 = x$, $u_2 = z_2 = y$, $u_3 = z_3 = z$, $u_4 = p_1 = p_x$, $u_5 = p_2 = p_y$, $u_6 = p_3 = p_z$, then $\dot{u}_i$ for $i = 1, 2, 3$ is given by Eq. (1) and $\dot{u}_i$ for $i = 4, 5, 6$ is given by Eq. (2). For the amplitudes of applied radiation considered in the present

study, the term of $-e\left(\mathsf{E}+\frac{\dot{\mathsf{z}}}{c}\times\mathsf{B}\right)$ could be safely ignored in Eq. (3) in comparison with the $-e^2\mathsf{z}/\left|\mathsf{z}\right|^3$ term, resulting in:

$$\mathsf{R}_{\rm reac}\approx-\frac{2}{3}\frac{e^4}{m^2c^3}\left[\frac{\mathsf{p}}{\left|\mathsf{z}\right|^3}-\frac{3\mathsf{z}(\mathsf{z}\cdot\mathsf{p})}{\left|\mathsf{z}\right|^5}\right] \quad . \tag{4}$$

(We estimate that the term ignored here is about a factor of $s\alpha^3$, or smaller, than the term retained, for the different radiation and orbit conditions considered in this article; here, s is a scaling factor we used that will be discussed more later, with its largest value used being 20, and $\alpha\approx 1/137$ is the fine structure constant. Hence, $s\alpha^3 \ . \ 10^{-5}$.)

In Ref. [1], we initially investigated a simple condition where a CP plane wave could precisely balance the radiation reaction of $\mathsf{R}_{\rm reac}$, for the situation where the orbiting charged particle followed a circular orbit. We now want to examine the analogous case where the charged particle follows a general elliptical orbit, which is the solution of the Keplerian equation of motion

$$m\ddot{\mathsf{z}}=-\frac{e^2\mathsf{z}}{\left|\mathsf{z}\right|^3} \quad , \tag{5}$$

if no radiation reaction and no applied radiation reaction was present. As solved in standard classical mechanics textbooks (see, for example, Refs. [18] or [19]), the solution to Eq. (5) is such that the particle stays in a single plane, and follows an elliptical orbit (see Fig. 2), with the radius described by:

$$r=\frac{\varepsilon P}{1-\varepsilon\cos(\theta)} \quad . \tag{6}$$

Here, θ is the polar angle, ε the eccentricity, and P is the distance from the focus to the directrix [20]. These parameters are related to the semimajor and semiminor axes, a and b, by

$$\varepsilon=\sqrt{1-\frac{b^2}{a^2}} \quad , \tag{7}$$

$$P=\frac{b^2}{\sqrt{a^2-b^2}} \quad . \tag{8}$$

The reverse relationships are: $a=\varepsilon P/(1-\varepsilon^2)$ and $b=\varepsilon P/\sqrt{1-\varepsilon^2}$. For an ellipse, ε ranges between $0\leq\varepsilon<1$, with $\varepsilon=0$ being the circular case, and $\varepsilon\to 1$ becoming extremely eccentric. In the circular limit of a fixed radius $a=b$, then $\varepsilon\to 0$ and $P\to\infty$ in such a way that $\varepsilon P\to a$, so $r\to a$ in Eq. (6).

The period for an elliptical orbit resulting from Eq. (5) is given by [18],[19]:

$$T=\frac{2\pi m^{1/2}a^{3/2}}{e} \quad , \tag{9}$$

which only depends on the semi-major axis a of the elliptical orbit.

For this nonrelativistic central force problem of Eq. (5), without radiation reaction and external electromagnetic forces acting, angular momentum is conserved, so $mr^2\dot{\theta} \equiv J$ is a constant. Moreover, by comparing the geometrical elliptical expression in Eq. (6) to the solution of Eq. (5), one can prove [18] that

$$J = mr^2\dot{\theta} = e\sqrt{m\varepsilon P} \quad . \tag{10}$$

From Eqs. (10) and (6):

$$\frac{d\theta}{dt} = \frac{e\sqrt{m\varepsilon P}}{m}\frac{[1-\varepsilon\cos(\theta)]^2}{(\varepsilon P)^2} \quad . \tag{11}$$

This can be integrated to obtain t as a function of θ (see integrals #2.5543 and #2.5533 on p. 148 in Ref. [21]):

$$\begin{aligned} t &= \frac{m(\varepsilon P)^2}{e\sqrt{m\varepsilon P}}\int_0^\theta d\theta' \left(\frac{1}{1-\varepsilon\cos\theta'}\right)^2 \\ &= \frac{m^{1/2}(\varepsilon P)^{3/2}}{e(1-\varepsilon^2)}\left\{\frac{\varepsilon\sin\theta}{(1-\varepsilon\cos\theta)} + \frac{2}{(1-\varepsilon^2)^{1/2}}\arctan\left[\frac{(1-\varepsilon^2)^{1/2}\tan\left(\frac{\theta}{2}\right)}{(1-\varepsilon)}\right]\right\} \quad . \end{aligned} \tag{12}$$

When $\varepsilon \to 0$ and $\varepsilon P \to a$ for circular motion, then the above reduces to $t = \theta/\omega$, with $\omega = 2\pi/T = e/(ma^3)^{1/2}$. Moreover, one can show that when $\theta = 2\pi$ in Eq. (12), then one obtains that

$$t(2\pi) = T = \frac{m^{1/2}(\varepsilon P)^{3/2}}{e(1-\varepsilon^2)}\left[\frac{2\pi}{(1-\varepsilon^2)^{1/2}}\right] \quad , \tag{13}$$

which agrees with Eq. (9) via Eqs. (7) and (8).

Figure 3 shows numerical evaluations of t/T as a function of θ [Eq. (12)] for various values of ε, for the region $0 \le t/T \le 1$ and $0 \le \theta/\pi \le 2$. (Since the motion is periodic, then continuing the plot for larger values of θ, simply corresponds to taking the plot of Fig. 3 and converting $\theta \to \theta + 2\pi n$ and $t \to t + nT$ for some integer n.) As can be seen for $\varepsilon = 0$, the circular case, the relationship is a linear one (straight line). As ε increases toward unity, the curve becomes very flat in the center region, with very steep sections at the beginning and end. To understand this physically, for a value of ε near unity, the ellipse in Fig. 2 would be extremely eccentric (small b/a ratio); for most of the orbit, the angular change of the orbit is extremely slow with respect to time, so a relatively long time is required for θ to change much. However, when the classical electron approaches point B in Fig. 2, which

is near the time $t = T/2$ on the $y-$axis in Fig. 3, then the angle changes very rapidly in a short amount of time, which is what gives rise to the near flat curve for $\varepsilon = 0.95$ in Fig. 3 near $t = T/2$.

III. CONDITION AND REALIZATION OF STABILITY

One of our main aims in the present article is to examine whether similar behavior occurs for elliptical orbits as did for the circular orbits in Ref. [1]. As expected, for the charged particle starting in an elliptic orbit, the orbit decays when no external radiation is applied, since the accelerated motion of the particle results in electromagnetic energy constantly being radiated away. Figures 4(a) and 4(b) show what happens to the classical charged particle, starting in an elliptical orbit with initial semimajor axis $a = 0.5$ Å, for a range of initial semiminor axis values and corresponding eccentricity values. As can be seen, we obtain the somewhat surprising result that these curves all become more circular ($\varepsilon \to 0$) as the orbit decays inward. Since all trajectories have the same initial value of a, then the initial periods of all these orbits are the same, namely, 1.396×10^{-16} sec, as given by Eq. (9). However, the rate of decay clearly increases as the initial eccentricity increases; nevertheless, all orbits tend to a circle.

We now turn to trying to find a condition where radiation can be directed at the elliptically orbiting charged particle to attempt to balance the radiation reaction. As will be shown, this can indeed be achieved, in principal, just as it was for the circular case. However, instead of one CP plane wave with a single frequency, now an infinite number of plane waves are required, of different amplitudes and phase relations, and of different harmonics associated with the main period of the orbit. The scheme we will take for doing this is exactly analogous to the situation in Fig. 1, but now with an infinite number of plane waves oriented in the $-\hat{\mathbf{z}}$ direction; our eventual task will be to find the appropriate distribution of amplitudes, phases, and frequencies, to accomplish this task. (Of course, a similar scenario can just as easily be worked out for radiation oriented along the $+\hat{\mathbf{z}}$ direction, provided appropriate changes in phase and polarization directions of the plane waves are also made.)

For Eqs. (1), (2), and (4) to reduce to Eq. (5), which is what yields an elliptical solution of the form of Eq. (6), we must have that the net Lorentz force from the applied radiation, which we will call $\mathbf{F}_{\rm Lor}$, must be equal and opposite to the radiation reaction of $\mathbf{R}_{\rm reac}$. Hence,

to find $\mathsf{F}_{\rm Lor}$ as a function of the position of the charged particle in its orbit, then we need to use Eqs. (4), (1), (2), (6), and (11), to obtain that

$$(\mathsf{F}_{\rm Lor})_x = -(\mathsf{R}_{\rm reac})_x = -\frac{1}{24}\frac{e^5}{m^{3/2}c^3\,(\varepsilon P)^{7/2}} \begin{bmatrix} (16 + 48\varepsilon^2 + 6\varepsilon^4)\sin(\theta) \\ -(48\varepsilon + 40\varepsilon^3)\sin(2\theta) \\ +(48\varepsilon^2 + 9\varepsilon^4)\sin(3\theta) \\ -20\varepsilon^3\sin(4\theta) + 3\varepsilon^4\sin(5\theta) \end{bmatrix} \quad , \tag{14}$$

$$(\mathsf{F}_{\rm Lor})_y = -(\mathsf{R}_{\rm reac})_y = -\frac{1}{24}\frac{e^5}{m^{3/2}c^3\,(\varepsilon P)^{7/2}} \begin{bmatrix} (16\varepsilon + 12\varepsilon^3) \\ -(16 + 48\varepsilon^2 + 6\varepsilon^4)\cos(\theta) \\ +(48\varepsilon + 32\varepsilon^3)\cos(2\theta) \\ -(48\varepsilon^2 + 7\varepsilon^4)\cos(3\theta) \\ +(20\varepsilon^3)\cos(4\theta) - (3\varepsilon^4)\cos(5\theta) \end{bmatrix} \quad , \tag{15}$$

where here it was assumed that the particle started on the semimajor axis at point A in Fig. 2, and traveled in the counterclockwise direction. As a check on the above expressions, we note that in the limit of a circular orbit, with $\varepsilon P \to a$ and $\varepsilon \to 0$, the above two expressions reduce to

$$(\mathsf{F}_{\rm Lor})_x = -\frac{2e^5}{3m^{3/2}c^3a^{7/2}}\sin(\theta) \quad , \tag{16}$$

and

$$(\mathsf{F}_{\rm Lor})_y = +\frac{2}{3}\frac{e^5}{m^{3/2}c^3a^{7/2}}\cos(\theta) \quad , \tag{17}$$

which agrees with Eqs. (8) and (9) in Ref. [1]. Thus, for circular motion, there is one harmonic, with $\theta = \omega t$, and $\omega = e/(mr^3)^{1/2}$, so one CP plane wave can provide the necessary force to balance the radiation reaction (in our nonrelativistic approximation). For elliptic motion, the necessary force in Eqs. (14) and (15) to accomplish this balancing requires trigonometric terms up through an order of five times θ; moreover, as seen in Eq. (12), for elliptical orbits, there no longer exists a linear relationship between t and θ, which brings in the need for an infinite number of harmonics in the radiation, which we turn to next.

Having obtained the correct condition required to balance the radiation reaction, we now turn to the harder task of finding the required radiation characteristics acting on the orbiting particle, to achieve this result. Undoubtedly there is more than one way to do this, at least in an approximate sense. We will choose the situation that most closely represents the case discussed for the circular case, as illustrated in Fig. 1. By having plane waves only traveling

in the $-\hat{\mathsf{k}}$ direction, then since B must be in the $x-y$ plane, the magnetic component of the Lorentz force, $(-e)\left(\frac{\dot{\mathsf{z}}}{c}\times\mathsf{B}\right)$, will act only in the $\hat{\mathsf{z}}$ direction when the particle orbits in the $x-y$ plane. Moreover, by running different simulation tests on the range of time and the conditions examined here, we found that ignoring this term had very little effect on the results we report here. Hence, we will ignore this term and treat it as a small secondary-order effect that may be important in some cases, but not for the situations reported here. (I.e., for very long simulations in time, the $(-e)\left(\frac{\dot{\mathsf{z}}}{c}\times\mathsf{B}\right)$ term would force the particle's orbit to change from a purely $x-y$ orientation, thereby changing the dynamics with the applied radiation considerably.)

Thus, to approximately achieve the desired stability condition, then $(-e)\,\mathsf{E}$ needs to equal Eqs. (14) and (15). The desired criteria, for points x in the $x-y$ plane, is that $\mathsf{E}(\mathsf{x},t+mT)=\mathsf{E}(\mathsf{x},t)$, where m is an integer; this way each orbit of the charged particle will experience the same repeated action, in precisely the same way. We know from Fourier analysis that to satisfy this condition, E can be expressed in the form (for x in the $x-y$ plane)

$$\mathsf{E}(\mathsf{x},t)=\sum_n \tilde{\mathsf{E}}_n(\mathsf{x})\,e^{-i\omega_n t}\quad , \tag{18}$$

where $\omega_n mT = N2\pi$, and m and N are integers. This condition is satisfied if

$$\omega_n = n\frac{2\pi}{T}\quad , \tag{19}$$

where n is an integer and ranges in Eq. (18) from $-\infty$ to ∞. Fourier analysis yields:

$$\tilde{\mathsf{E}}_n(\mathsf{x})=\frac{1}{T}\int_0^T dt\mathsf{E}(\mathsf{x},t)\exp\left[\frac{2\pi int}{T}\right]\quad , \tag{20}$$

where here $\mathsf{E}(\mathsf{x},t)$, for x in the $x-y$ plane, would be set equal to $\frac{1}{(-e)}\mathsf{F}_{\rm Lor}$ in Eqs. (14) and (15). Now, $\mathsf{F}_{\rm Lor}$ has been expressed in terms of θ, which in turn is related to t via Eq. (12). It should be noted that $\mathsf{E}(\mathsf{x},t)$ only depends on z and t, and not on x and y, since $\mathsf{E}(\mathsf{x},t)$ is composed here of plane waves moving in the $-\hat{\mathsf{z}}$ direction. Hence, for x in the $x-y$ plane:

$$\tilde{\mathsf{E}}_n(\mathsf{x})=-\frac{1}{eT}\int_0^{2\pi} d\theta'\frac{dt}{d\theta'}\mathsf{F}_{\rm Lor}(\theta')\exp\left[\frac{2\pi int(\theta')}{T}\right]\quad . \tag{21}$$

By making use of Eqs. (14), (15), (12), and (13), then Eq. (21) can be numerically obtained, for specified values of a and ε.

Several properties can be analytically proven for $\tilde{\mathsf{E}}_n$. Since $\mathsf{E}(\mathsf{x},t)$ must be real, then $\tilde{\mathsf{E}}_{-n} = \tilde{\mathsf{E}}_n^*$. Also, based on the following property that $\theta(-t) = -\theta(t)$ (assuming $\theta(t) = 0$), and recognizing from Eqs. (14) and (15) that $F_x(-\theta) = -F_x(\theta)$ and $F_y(-\theta) = +F_y(\theta)$, then one can show that $\tilde{E}_{x,-n} = -\tilde{E}_{x,n}$ and $\tilde{E}_{y,-n} = +\tilde{E}_{y,n}$. Consequently, $\tilde{E}_{x,n}^* = -\tilde{E}_{x,n}$, so $\tilde{E}_{x,n}$ is an imaginary quantity, and $\tilde{E}_{y,n}^* = \tilde{E}_{y,n}$, so $\tilde{E}_{y,n}$ is a real quantity.

Figures 5(a) through 5(f) show plots of numerical values calculated for $E_{x,n}$ and $E_{y,n}$ for three values of ε, namely, 0.1, 0.5, and 0.9, with $a = 0.5$ Å. As expected, for a low value of ε, namely $\varepsilon = 0.1$ in Figs. 5(a) and (b), then only the first few values of $\tilde{\mathsf{E}}_n$ are appreciable. As $\varepsilon \to 0$, the stability condition should reduce to the circular case discussed in Ref. [1], where only the $n = 1$ and $n = -1$ coefficients are nonzero. As can be seen in Figs. 5(a) and 5(b), where $\varepsilon = 0.1$, the $n = 1$ coefficient, times two (to convert to sine and cosine amplitudes), is indeed close in value to the circular orbital value, with $a = 0.5$ Å, of 5.419 statvolt value discussed in Ref. [1]. As ε increases toward unity, more and more harmonics become necessary to enable the incident radiation to balance the radiation reaction. For the $\varepsilon = 0.9$ case shown in Figs. 5(e) and (f), harmonics through order $n \approx 200$ are clearly appreciable.

It's hard not to notice the intriguing shape of the envelope of the spectral coefficient histograms shown in Fig. 5, as it looks so much like the character of a blackbody radiation spectral curve. More will be said about this suggestive, but totally speculative observation, in the concluding section of this article. For now, we simply note that as ε increases toward unity, the maximum of this envelope curve steadily moves to the right, just as the peak of a blackbody radiation curve moves to the right as temperature increases. Even at the value of $\varepsilon = 0.5$ in Figs. 5(c) and (d), the peak value has moved significantly from the first harmonic position to the positions of $n = 3$ and 4; for $\varepsilon = 0.9$, the peak has moved to $n = 48$. Moreover, as seen in the plots, besides the peak position moving to the right to higher harmonic values as ε increases, so also the maxima of $|E_{n,x}|$ and $|E_{n,y}|$ in these plots increases as $\varepsilon \to 1$, just as happens for the peak of the Planckian spectrum (without zero-point) as the temperature increases.

As should be expected, when the condition of Eq. (21) is satisfied for all n, then the radiation reaction becomes balanced and the elliptic orbit will be maintained without decay. We have carried out numerical simulation experiments that show this works fairly well if not all the harmonics are retained, but rather a cutoff is introduced, so that the very high

frequency, but low amplitude, components are ignored. A variation is then introduced in the simulations, that becomes smaller as more harmonics are included, as one might expect.

Figures 5(g), 5(h), and 5(i) show what happens as more and more harmonics are included in the simulation for the situation where the orbiting particle's initial orbit is characterized by $a = 0.5$ Åand $\varepsilon = 0.5$. The notation in these figures means, for example, when $n = 10$, then harmonics up to order $n = 10$ are included in the simulation, where the values of the amplitudes of the plane waves are as found in Figs. 5(c) and 5(d). As expected, the more harmonics, the closer the curves come to the perfect balance situation where a, b, and ε remain constant. It is interesting to observe in the present situation, that for a finite number of harmonics included, one still observes an initial near-stable condition, with the decay point moving farther and farther out in time as n increases.

The remainder of this article does not use this plane wave representation, but approaches the analysis from a different point of view that will be discussed next. We note, however, that the simulations described in the next section have in many cases also been checked by the plane wave analysis just mentioned. In general, there seems to be good agreement, with the agreement improving as more harmonics are included.

IV. NUMERICAL STUDY INVOLVING MORE COMPLEX STABILITY CONDITIONS

The question of achieving perfect balance between the effects of applied radiation and radiation reaction on the orbiting particle is of course interesting, but, seemingly rather contrived and very specific. A more interesting question concerns the orbital behavior if the radiation is scaled either above or below this specific balance condition. As shown in Ref. [1], when the CP wave amplitude was increased above this critical value, then a stability was still obtained, but with a very pronounced periodic variation in the radius versus time plot; the variation amplitude increased as the CP amplitude increased, while the period of this radial variation decreased. A very large range of amplitudes above this critical-balancing amplitude of the CP wave resulted in this stability-like behavior.

The natural question arises as to whether this same scenario might hold for elliptical orbits. Let us again consider the situation in Fig. 1, with radiation directed in the $-\hat{\mathbf{z}}$ direction from a source of light at the point $R\hat{\mathbf{z}}$. If the distance R is much larger than

the aperture of the light source, then the light source can be nicely represented as a sum of spherical waves, of different wavelengths. The wavelengths required to achieve the radiation reaction balance condition are given by $\lambda_n = cT/n$, $n = 1, 2, ...$, where T is the period of the orbiting particle. For $R \gg cT = \lambda_1$, the effect of the spherical waves on the orbiting particle will be indistinguishable from the effect of plane waves acting. Moving the source closer or farther away from the $z = 0$ plane results in the amplitudes of these effective plane waves changing in accordance with the factor of $1/R$, which governs the magnitude of the spherical wave amplitudes in the long distance, radiation zone.

Hence, it seems reasonable to examine the condition where all the effective plane wave amplitudes are increased or decreased by the same corresponding factor. Our physical picture to achieve this condition consists of simply moving the source of light closer or farther from the classical hydrogen-like system.

To simulate these conditions, however, there are two steps we found important to make. First, although the use of a sum of plane waves certainly does work, still, for very long simulation runs, not knowing whether the deviations in curves are due to predicted physical effects, or due to not accurately representing the applied radiation via a finite number of plane waves, seemed an important step to overcome. Hence, we decided to use $\mathsf{E} = s\left(\frac{1}{-e}\right)\mathsf{F}_{\rm Lor}$, with $\mathsf{F}_{\rm Lor}$ given by Eqs. (14) and (15), and s is a positive scaling factor ($s = 1$ is the balance condition for the radiation reaction) as a more compact way of representing the electric field of the applied radiation acting on the orbiting $(-e)$ particle in the $x - y$ plane. To make use of this relationship, $\mathsf{F}_{\rm Lor}$ needs to be expressed in terms of t, rather in terms of θ. But, except for the trivial case of $\varepsilon = 0$, we do not have an analytic means of expressing θ in terms of t; rather, we only seem to be able to express t in terms of θ via Eq. (12), but not the inverse.

We should note that for $s = 1$, the particle will be forced to remain in a perfectly elliptical orbit (at least in the present nonrelativistic treatment). For this specific case, then θ in Eqs. (14) and (15) represents the angular position of the particle in the elliptical orbit. For $s \neq 1$, the particle will not stay in an elliptical path, but will deviate from it; eventually the orbit will decay, thereby changing significantly from the initial elliptical orbit. Hence, for $s \neq 1$, the parameter θ in Eqs. (14) and (15) will not be the true angular position of the particle; instead, it represents the angular position of a particle if it was to maintain the initial elliptical orbit. This distinction is somewhat subtle, but quite critical.

Thus, we can simulate different radiation conditions that scale the balanced radiation by a factor s, by using the following relationship, for points x in the $x-y$ plane ($z = 0$):

$$\mathsf{E}(\mathsf{x}, t) = s\left(\frac{1}{-e}\right)\mathsf{F}_{\rm Lor}\left[\theta_{s=1}(t)\right] \quad , \tag{22}$$

where we use as the argument of $\mathsf{F}_{\rm Lor}$ not the true angular position of the particle (for $s \neq 1$), but rather the angular position that would have been the situation in the constant elliptical case of $s = 1$, with $\theta_{s=1}(t)$ being the inverse of Eq. (12). [To better clarify what we mean in Eq. (22), the quantity $\mathsf{F}_{\rm Lor}\left[\theta_{s=1}(t)\right]$ is precisely the force exerted by the plane waves if perfect orbital balance could be maintained, and $\left(\frac{1}{-e}\right)$ times this quantity is the net electric field of the plane waves, at time t in the $x-y$ plane, to achieve this perfect balance. If we consider another radiation condition that has a scaled value of this electric field, by a fixed factor s, then we obtain the expression of Eq. (22). Again, there are many physical ways that one might achieve this radiation condition, but, a very natural way would be by simply moving the source of light farther from or closer to the atom, along the $\hat{\mathsf{z}}$ direction.]

We can find $\theta_{s=1}(t)$ numerically. A very convenient and accurate way of doing so that managed to fit in nicely with our specific numerical implementation using the Bulirsch-Stoer method with an adaptive step control [22], was is to add another variable, $u_7 \equiv \theta_{s=1}(t)$ to the six variables solved for in our scheme. Specifically, we used $u_1 = x(t)$, $u_2 = y(t)$, $u_3 = z(t)$, $u_4 = p_x(t)$, $u_5 = p_y(t)$, $u_6 = p_z(t)$, with $\dot{u}_i$ for $i = 1, 2, 3$ given by Eq. (1), $\dot{u}_i$ for $i = 4, 5, 6$ given by Eq. (2), and with $\varepsilon P = a(1-\varepsilon^2)$ in Eq. (11),

$$\dot{u}_7 = \frac{e}{\sqrt{m}a^{3/2}(1-\varepsilon^2)^{3/2}}\left\{1 - \varepsilon\cos\left[\theta_{s=1}(t)\right]\right\}^2 \quad . \tag{23}$$

In turn, the $\dot{u}_4$, $\dot{u}_5$, and $\dot{u}_6$ first-order differential equations from Eq. (2) became:

$$\dot{\mathsf{p}} = -\frac{e^2\mathsf{z}}{|\mathsf{z}|^3} + \mathsf{R}_{\rm reac} + s\mathsf{F}_{\rm Lor}\left[\theta_{s=1}(t)\right] \quad , \tag{24}$$

where p, z, and $\theta_{s=1}$ should be replaced by the associated u_i quantities for $i = 1, 2, ..., 7$, and where $\mathsf{R}_{\rm reac}$ was expressed by Eq. (4). For our nonrelativistic treatment, and ignorance of the magnetic component of the Lorentz force for the time lengths we simulated, the above scheme can be simplified by substituting $\dot{u}_3 = \dot{z} = 0$, and $\dot{u}_6 = \dot{p}_z = 0$, thereby forcing the particle's orbit to remain in the $x-y$ plane of $z = 0$. However, without this restriction, the above scheme clearly can hold in general for the full 3-D motion; we anticipate such

effects will be important in future work, particularly when longer time durations involving relativistic speeds may become critically important.

The second step we found important to make, to be able to report accurate numerical results, was to find a reasonable approach for extracting elliptical parameters of a, b, and ε (of course, only two of these three parameters are required, but all three are interesting to examine) from the classical electron's motion. As in Fig. 4, we anticipate the orbiting motion to be approximately elliptical at any moment, but the approximate semimajor and semiminor axes will slowly change with time. We found a convenient way to represent this was to generalize Eq. (6) slightly, to

$$r\,(\theta) \;=\; \frac{a\,(1-\varepsilon^2)}{1-\varepsilon\cos\left[\theta-\theta_0\right]} \quad , \tag{25}$$

where again $a\,(1-\varepsilon^2) = \varepsilon P$, and where θ_0 is a parameter that represents the initial starting angle of an elliptical orbit. The relationships of $x = r\cos(\theta)$ and $y = r\cos(\theta)$ still hold of course. The effect of θ_0 is to tilt the ellipse shown in Fig. 2, so that the semimajor axis becomes tilted at an angle θ_0 with respect to the $x-$axis. By keeping track of r and θ values of the orbiting particle, for N points, where we would make N large enough to encompass at least one or more orbits, then the parameters a, ε, and θ_0 could be adjusted to curve-fit the simulated data for every few orbits. Specifically, the way we did this was to re-express Eq. (25) via

$$\frac{1}{r} \;=\; \frac{1}{a\,(1-\varepsilon^2)} - \left[\frac{\varepsilon\cos(\theta_0)}{a\,(1-\varepsilon^2)}\right]\cos(\theta) - \left[\frac{\varepsilon\sin(\theta_0)}{a\,(1-\varepsilon^2)}\right]\sin(\theta) \quad . \tag{26}$$

By making a table of $1/r$, $\cos(\theta)$, and $\sin(\theta)$ for N points, then the parameters $\frac{1}{a(1-\varepsilon^2)}$, $-\frac{\varepsilon\cos(\theta_0)}{a(1-\varepsilon^2)}$, and $-\frac{\varepsilon\sin(\theta_0)}{a(1-\varepsilon^2)}$ can be obtained by conventional least-squares methods, since these parameters appear linearly in the above relationship. From these three extracted parameters, a, ε, and θ_0 were obtained; b and P could then be easily obtained from a and ε. Although not mentioned earlier, in fact Figs. 4a and 4b, for the $s = 0$ case, were obtained precisely in this way.

Figures 6(a) through 6(d) show some of our simulation results using this strategy. Figure 6(a) superimposes plots of a and b versus time, for orbits all beginning with the same initial value of $a = 0.5$ Å and the same eccentricity of $\varepsilon = 0.5$, or $b = a\sqrt{1-\varepsilon^2} \approx 0.433$ Å. Radiation corresponding to Eqs. (18) and (21), but as multiplied by different scale factors, s, is assumed to be present that influences the motion of the orbiting particle. Situations

for scale factors of $s = 0$, 1, 2, 5, 10, 15, and 20 are shown. [These factors were chosen to help correspond with the interesting results found for the circular case in Ref. [1] of Fig. 3(a). In that figure, the $A = 5.419$ statvolt case corresponds to the $s = 1$ case analyzed here, and the $A = 100$ statvolt case roughly corresponds to the $s = 20$ case here.] The $s = 0$ case is simply the base case with no radiation present, while the $s = 1$ case is where the radiation reaction is perfectly balanced. Nothing new exists for these two situations than what has already been described so far. However, for $s =$2, 5, 10, 15, and 20, we obtain the intriguing results of extended stability, but with eventual decay. Decay always results in the orbits tending to a circular one, as indicated by the corresponding plots of ε versus time in Fig. 6(b) (all orbits, after starting the decay trend, asymptotically reach $\varepsilon = 0$). Somewhat surprisingly, the semimajor axis tends to be far more stable than the semiminor. As seen in Fig. 6(a), for $s = 2$, 5, and 10, b increases at first, as though tending toward a, before eventually decaying.

Figure 6(c) zooms in on the early behavior of a vs. t. The behavior seen here corresponds closely to the behavior seen in the circular case, as shown in Fig. 3(a) in Ref. [1]. As the radiation is scaled in magnitude above the balance condition of $s = 1$, a different sort of stability arises, consisting of a periodic pattern of spiraling outward and inward motion of the orbiting particle. As with the circular case, as the scale of the radiation increases, the amplitude of the periodic ripples in a and b in Figs. 6(c) and 6(d) increase, while the period of these ripples decreases. It should again be emphasized that in each of the periodic ripples shown in Fig. 6(c), the classical electron is executing a huge number of orbits. Since the period of each orbit is about 1.4×10^{-16} sec, then about 3600 orbits are contained in the plots of Figs. 6(c) and 6(d). The very stable behavior of a in Fig. 6(c) looks very much like the circular case. The zoomed-in view of b vs. t in Fig. 6(d) shows that the semiminor axis is certainly far more stable than the "no-radiation" case ($s = 0$), but, the center of the envelope curve is not flat, as in the semimajor axis situation. This result came as a surprise to us.

Figure 7(a) zooms in on Fig. 6(a) to more clearly show that decay sets in at the same time for every pair of a and b versus t curves; the centers of the envelopes of the a vs. t curves are clearly very flat until decay occurs, while the centers of the envelopes of the b vs. t curves have a curve to them. Figures 7(b) and 7(c) zoom in even more on the a vs. t and b vs. t curves to show that the envelope curves continue to widen, until decay finally

sets in. The larger the value of s, the faster the envelope curves widen. This fact is easy to notice in Fig. 7(b), but, a close examination of Fig. 7(c) shows that it holds true for the semiminor axes as well. Figure 7(b) is similar to Fig. 6(b) for the circular case in Ref. [1]. Figures 7(d) and 7(e) zoom in on the transition point for the $s = 20$ curves for the a and b axes, respectively; the widening of the envelope curves can be seen slightly here as well.

Perhaps one of the most surprising aspects of the $s > 1$ situations, is that the semimajor and semiminor axes slowly rotate with respect to their initial position. This is revealed by Fig. 8(a). For $s > 1$, a net torque results in the counterclockwise direction that acts on the orbiting particle; this torque occurs because the applied radiation exerts a greater force than does the radiation reaction. Interestingly, once decay sets in, and the orbit begins to decrease, then θ_0 stays essentially constant. We attribute this effect to the fact that once the orbit begins to decrease, then the period of the orbit decreases, and the resonance like effect of the applied radiation at the initial period of the orbit diminishes enormously. We placed a small circular point on each of the curves in Fig. 8(a) to indicate where transitions to orbital decay began; as can be seen, to the right of each such point, the θ_0 vs. t curve is essentially flat. It is very interesting to see how the pattern of marked transition points proceeds as s increases in size. To help aid this view, arrows from each transition marked point to another are shown.

For $s = 0$ and $s = 1$, the semimajor and semiminor axes in Fig. 8(a) clearly remain oriented along the x and y axes, respectively. Moreover, for $0 < s < 1$, θ_0 remains nearly zero, with a very slight noisy variation that can only be observed when zooming in on the region. (We believe the origin of the noise to simply be the least square procedure of a finite number of data points, fit to an orbit with θ_0 nearly equal to zero.) For increasing values of s, for $0 \leq s \leq 1$, the end points of the θ_0 vs. t curves in Fig. 8(a) move farther and farther to the right of the point indicated as "$s = 0$ ends;" for $s \to 1$ this "end" point should go to infinity.

Figures 8(b), 8(c), and 8(d) show, respectively, ε vs. t, a vs. t, and b vs. t, for a wide range of values of s. A brief amount of studying of these plots enables one to deduce the patterns of these orbital parameters as s increases in value. Again, we placed small circular points to indicate where the orbits changed to ones of a decaying pattern.

Figures 9(a), 9(b), and 9(c) show what happens when s is slightly less than unity. The a vs. t, b vs. t, and ε vs. t curves all have a very similar character. The closer s is to

unity, the longer the curves hug the related $s = 1$ curve, before eventually decaying; thus, the decay point in time increases toward infinity as s approaches unity.

V. CONCLUDING REMARKS

Here we reported simulation results for a classical charged-point particle, with charge $-e$, in near-elliptical orbits around a classical $+e$ charged, infinitely massive nucleus. This work naturally extends the analysis on this same system for near-circular orbits in Ref. [1]. The present elliptical study involves some interesting new complexities, but, many of the same patterns seen in the near-circular case are again revealed here. In particular, a balancing-radiation condition can be established that essentially negates the effects of the radiation reaction. However, whereas in the circular case only one CP plane wave was required to accomplish this task, in the elliptical case an infinite number of plane waves are required, consisting of all the harmonics of the period of the orbit. The larger the ellipticity of the orbit, the more significant becomes the contribution of the higher frequency components in the applied radiation to assure a near stability condition. Figure 5 shows the interesting behavior of the required radiation spectrum needed to achieve a balance, for several values of eccentricity, ε.

The key nonlinear effects that are similar to those in the near-circular case, occur when the radiation required for balancing the orbit, is scaled by a factor greater than unity. A stability-like behavior results, where the semimajor and semiminor axes, a and b, spiral in and out in magnitude, before eventually falling into a decaying situation where the radiation reaction becomes completely dominate. The behavior of a is very similar to the radius in the near circular case, as seen in Figs. 6(a) and 6(c); as the scaling factor, s, becomes larger, the amplitude of the periodic spiraling in and out motion becomes larger, while the period of the spiraling behavior becomes smaller. The behavior of b is somewhat analogous, but it is also quite different. Although b spirals in and out, with an amplitude that increases and a period that decreases the larger the value of s, the center of the envelope of this spiraling behavior does not remain flat, as it does for the semimajor axis. Instead, significant changes in the center occur, that are dependent on the value of s. Figures 6(a) and 6(d) show these points. Moreover, the envelopes of these curves become wider with time, until decay sets in. At this point, the phases of the motion of the orbiting particle and the radiation become

too different for balancing to occur; radiation reaction then results in a swift change to a decaying orbit. Figure 7 shows these effects.

Besides the unexpected behavior of the envelope of the semiminor axis, there are several other effects that should be emphasized. First, as noticed in the very beginning of the study without the effects of applied radiation acting, an initially eccentric orbit decays, with $\varepsilon \to 0$. Thus, initial elliptical orbits become more and more circular as the decay progresses. Figure 4 shows this effect. Moreover, eccentric orbits that have been maintained in stability due to applied radiation, as shown in Figs. 6a and 6b, still have the orbits eventually decay toward a circular orbital shape as $r \to 0$. It will be interesting to fully investigate what sort of effect relativistic corrections have on this behavior.

Another somewhat unexpected result is that the orientation of a and b with respect to the $x-$ and $y-$axes, begins to rotate when $s > 1$. Figure 8 shows this effect. We attribute this effect to the net torque exerted on the orbiting particle that is larger than the opposing one due to the radiation reaction.

As shown in Figs. 5(a)-(f), the Fourier plane wave contributions required to maintain stability for elliptical orbits have a shape and behavior, as $\varepsilon \to 1$, that is reminiscent of the properties of a blackbody radiation spectra as temperature increases. Moreover, an interesting idea arises if one combines this observation with the earlier observation that the radiation reaction term in the Lorentz-Dirac equation acts to make elliptical orbits tend toward circular ones. Now, a key original aim of SED was to show that a full accounting for the dynamic interaction of zero-point plus Planckian radiation, together with a classical charged particle in a Coulombic binding potential, would yield a thermodynamically stable system [13],[14],[15],[16]. To date, research on SED has not successfully shown this to be the case. If it did, however, then the following idea might be plausible, namely: the higher the temperature, the more likely the probability of finding elliptic-like orbits; conversely, the lower the temperature, the greater the likelihood for finding distributions of more circular-like orbits. Such statements are in some ways quite naive, since any sort of "orbit" must be extremely ragged as more and more high frequency components of zero-point plus Planckian radiation are taken into account; however, perhaps the probability distribution of "central" paths of the ragged motion may have a character that behaves in the way just described.

As for future work, we believe that are a number of interesting effects that should be examined that potentially have theoretical interest for SED and for classical and semiclassical

physics. Moreover, we believe that there are practical applications of the present study. By tailoring the time variation of applied electromagnetic radiation on Rydberg-like atoms, then some very unusual behaviors should be realizable, that have only moderately been examined in the past by experimentalists.

The present treatment has been a nonrelativistic approximation. Clearly, as the radius becomes smaller, and the speed becomes higher, then a relativistic treatment should become critical. Consequently, most of the present work focused on the orbiting behavior at radii large enough to not require this treatment. However, when the orbit decays sufficiently, then our work should be corrected and plots like Fig. 4(a), where $r \to 0$, will need to be altered for $r \lesssim 0.1$ Å, particularly when one zooms in on these regions in such plots. For the scale of the plots we have shown, we have not seen much of an effect, but, clearly if one examines applied radiation that corresponds to the frequency of an orbiting particle with $a \lesssim 0.1$ Å, then a relativistic treatment will become critical. Our present article has not considered such cases.

We intend to report on some of these relativistic effects, as well as examine numerical simulation experiments to attempt to make rapid jump-like effects occur in average orbital parameters. Finally, future work will begin to study the effects of multiple frequencies of applied radiation that are off-resonance from the orbit, with the goal being to better take into account, or at least better understand, the effects of a continuous spectrum of radiation acting on a classical orbiting charged point particle in a Coulombic binding potential.

Acknowledgement

We thank Prof. Timothy Boyer for reading the preprint of this article and for his helpful suggestions and encouragement.

---

[1] D. C. Cole and Y. Zou. Simulation study of aspects of the classical hydrogen atom interacting with electromagnetic radiation: Circular orbits. Journal of Scientific Computing, 2003. , to be published Vol. 18, No. 3, June, 2003.

[2] J. Grochmalicki, M. Lewenstein, and K. Rzazewski. Stabilization of atoms in superintense laser fields: Is it real? Phys. Rev. Lett., 66(8):1038–1041, 1991.

[3] J. A. Griffiths and D. Farrelly. Ionization of rydberg atoms by circularly and elliptically polarized microwave fields. Phys. Rev. A, 45(5):R2678–R2681, 1992.

[4] P. A. Braun. Discrete semiclassical methods in the theory of rydberg atoms in external fields. Rev. Mod. Phys., 65(1):115–161, 1993.

[5] W. Clark and C. H. Greene. Adventures of a rydberg electron in an anisotropic world. Rev. Mod. Physics, 71(3):821–833, 1999.

[6] S. Yoshida, C. O. Reinhold, P. Kristofel, and J. Burgdorfer. Exponential and nonexponential localization of the one-dimensional periodically kicked rydberg atom. Phys. Rev. A, 62:023408, 2000.

[7] C. Wesdorp, F. Robicheaux, and L. D. Noordam. Displacing rydberg electrons: The monocycle nature of half-cycle pulses. Phys. Rev. Lett., 87(8):083001, 2001.

[8] T. F. Gallagher, R. M. Hill, and S. A. Edelstein. Method and apparatus for field ionization for isotope separation. US Patent No. 4,070,580; see: www.uspto.gov, pages 1–7, 1978.

[9] R. Bir and J. P. Schermann. Method of isotope separation. US Patent No. 4,360,501; see: www.uspto.gov, pages 1–6, 1982.

[10] T. Oomori, K. Ono, and S. Fujita. Ion current generator system for thin film formation, ion implantation, etching and sputtering. US Patent No. 4,893,019; see: www.uspto.gov, pages 1–43, 1990.

[11] T. Oomori and K. Ono. Ion source. US Patent No. 5,115,135; see: www.uspto.gov, pages 1–75, 1992.

[12] L. D. Noordam and M. D. Lankhuijzen. Apparatus for detecting a photon pulse. US Patent No. 6,049,079; see: www.uspto.gov, pages 1–9, 2000.

[13] D. C. Cole. Reviewing and extending some recent work on stochastic electrodynamics. pages 501–532. World Scientific, Singapore, 1993.

[14] L. de la Peña and A. M. Cetto. The Quantum Dice - An Introduction to Stochastic Electrodynamics. Kluwer Acad. Publishers, Kluwer Dordrecht, 1996.

[15] T. H. Boyer. Random electrodynamics: The theory of classical electrodynamics with classical electromagnetic zero–point radiation. Phys. Rev. D, 11(4):790–808, 1975.

[16] T. H. Boyer. The classical vacuum. Sci. American, 253:70–78, August 1985.

[17] T. Uzer, D. Farrelly, J. A. Milligan, P.E. Raines, and J. P. Skelton. Celestial mechanics on a microscopic scale. Science, 253(42):42–48, 1991.

[18] R. A. Becker. Introduction to Theoretical Mechanics. McGraw-Hill, New York, 1954.

[19] H. Goldstein. Classical Mechanics. Addison–Wesley, Reading, MA, second edition, 1981.

[20] H. B. Fine and H. D. Thompson. Coordinate Geometry. The Macmillan Company, Norwood, MA, 1918.

[21] I. S. Gradshteyn and I. M. Ryzhik. Tables of Integrals, Series, and Products,, page 312. Academic, New York, 1980. #3.3551.

[22] W. H. Press, S. A. Teukolsky, W. T. Vetterling, and B. P. Flannery. Numerical Recipes in C: The Art of Scientific Computing. Cambridge University Press, New York, second edition, 1992.

Figure Captions

Figure 1: Sketch of situation examined in Ref. [1], with a CP plane wave directed in the $-\hat{\mathsf{z}}$ direction on a classical charged particle, with charge $-e$, orbiting in a circular motion in the $x-y$ plane. The same sketch holds for the present article, but with the orbit now an ellipse as in Fig. 2, and the radiation similarly directed, but consisting of an infinite number of plane waves of different frequencies.

Figure 2: Diagram of ellipse. a is the semimajor axis, b is the semiminor, θ the polar angle, and ε the eccentricity. For the simulations presented here, the orbits all begin with the classical electron at point A, traveling in the counterclockwise direction. The classical nucleus resides at point C. At point A (B), the classical electron is at the farthest (closest) point to the classical nucleus.

Figure 3: Numerical evaluations of $t\,(\theta)$ in Eq. (12), normalized by the period T in Eq. (9) for various values of ε.

Figure 4: (a) Plots of a and b (semimajor and semiminor) axes as a function of time, for the situation where the orbiting charged particle starts in an initial elliptical orbit, with $a\,(t = 0) = 0.5$ Å, for various values of eccentricity ε, as indicated next to each set of two curves. Only radiation reaction is assumed to be acting here. The semiminor axes are dotted lines. For $\varepsilon = 0$, then $a = b$. For $\varepsilon = 0.1$, a and b are still nearly on top of each other at this scale, so the two curves appear as a single one in this figure. For all other values of ε shown, the pair of two curves is clearly discernible. (b) ε plotted a function of time, under the same conditions. The starting values of ε used for the five curves shown were $\varepsilon = 0.1$, 0.3, 0.5, 0.7, and 0.9. For each curve, $\varepsilon \to 0$, then circular case.

Figure 5: (a) through (f) are histograms of $\tilde{E}_{x,n}/i$ ($\tilde{E}_{x,n}$ is pure imaginary) and $\tilde{E}_{y,n}$ (real quantity), as numerically calculated using Eq. (21) for various values of ε, all with $a = 0.5$ Å. (a) $\tilde{E}_{x,n}/i$ for $\varepsilon = 0.1$; (b) $\tilde{E}_{y,n}$ for $\varepsilon = 0.1$; (c) $\tilde{E}_{x,n}/i$ for $\varepsilon = 0.5$; (d) $\tilde{E}_{y,n}$ for $\varepsilon = 0.5$; (e) $\tilde{E}_{x,n}/i$ for $\varepsilon = 0.9$; (d) $\tilde{E}_{y,n}$ for $\varepsilon = 0.9$. Figures (g), (h), and (i) examine the initial $\varepsilon = 0.5$, $a = 0.5$ Åcase, as more and more harmonic are included in the simulation. Specifically, plots of (g) a vs. t, (h) b vs. t, and (i) ε vs. t, are shown, where in each plot first the "no plane wave case" is shown ($n = 0$ curve), then subsequent curves where harmonics up to order n are included. As expected, with more harmonics, the closer the curves come to the predicted perfect balance situation.

Figure 6: (a) Semimajor (solid curves), a, and semiminor (dashed curves), b, axes vs. t, for radiation scaling conditions of $s = 0$ (no radiation), $s = 1$ (precise radiation reaction balancing condition), and $s = 2$, 5, 10, and 20 ; (b) eccentricity, ε, vs. t for the same conditions as in (a); (c) zoom-in view of a vs. t in the early quasi-stable region, with only the $s = 0, 1, 2, 20$ curves shown here, to improve clarity. The trend for the other values of s is analogous. (d) zoom-in view of b vs. t in the early quasi-stable region. In addition to $s = 0, 1, 2, 20$, $s = 10$ is also displayed to help show the trend. As s increases above unity, the b vs. t curves tend to rise ($s = 2, 10$), but when s becomes too large ($s = 20$) then the curve falls.

Figure 7: These figures examine more about the decay points of the quasi-elliptical orbits. (a) zoom-in view of 6(a) to show that decay occurs at the same point for every pair of a vs. t and b vs. t curves; (b) zoom-in view of a vs. t for the regions where the curves are quasistable, before leading into decay. The large black regions exist because of the large number of fluctuations of a vs. t. At the scale shown here, the envelopes of the curves are clearing discernible, each increasing in width until decay finally occurs. Several figures here show various blown-up examinations of the blackened regions, such as the early time region in Fig. 6(c). (c) zoom-in view of b vs. t for the regions where the curves are quasistable, before decaying; (d) zoom-in view of a vs. t for the $s = 20$ case, near the point where decay occurs; (e) zoom-in view of b vs. t for the $s = 20$ case, near the point where decay occurs.

Figure 8: These plots show how the patterns evolve as s increases from 0 to 20 for the following quantities: (a) θ_0 vs. t, in Eq. (25); (b) ε vs. t; (c) a vs. t; and (d) b vs. t. Small circular points were place to help indicate where transitions to orbital decay began. The arrows from one circular point to another proceed from $s = 0$ to $s = 20$. The pattern for the a vs. t curves, as s increases, is fairly easy to identify, so additional markers were not placed in Fig. 8(c). The initial starting point for all orbits indicated in these plots was $a = 0.5$ Åand $\varepsilon = 0.5$.

Figure 9: These figures examine the situation as s approaches $s = 1.0$. (a) a vs. t; (b) b vs. t; (c) ε vs. t. The closer s is to 1.0, the longer stability lasts before decay sets in. After decay sets in, the curves parallel the slope of the $s = 0$ (no radiation) curve.

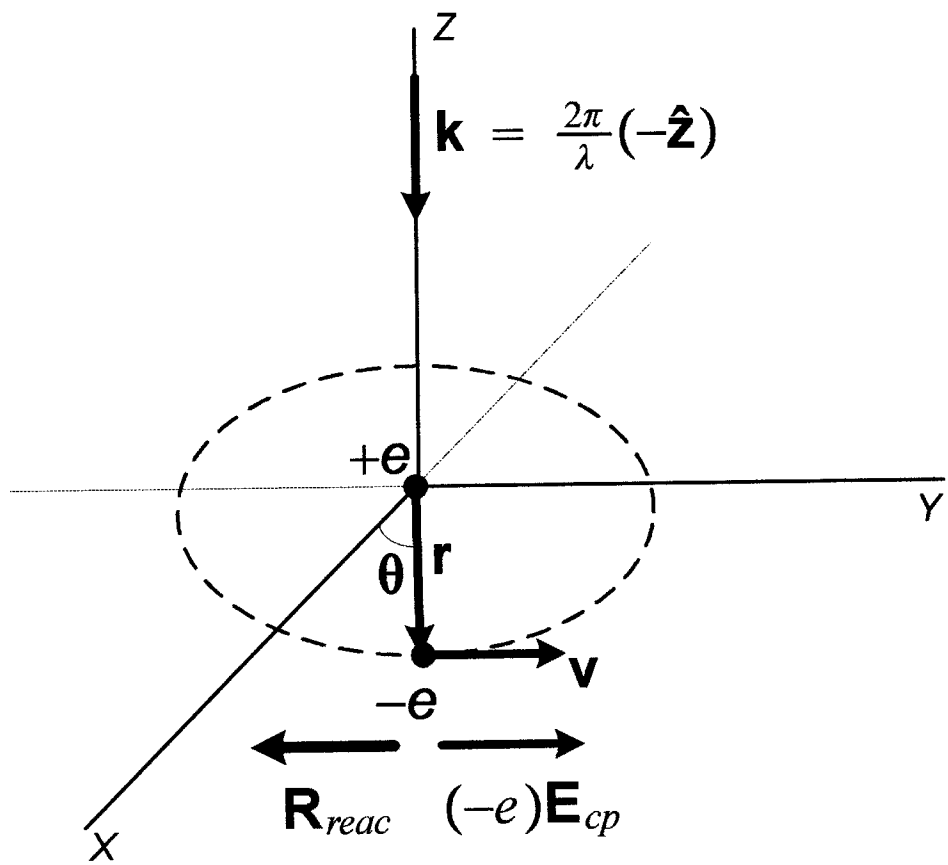

Fig. 1

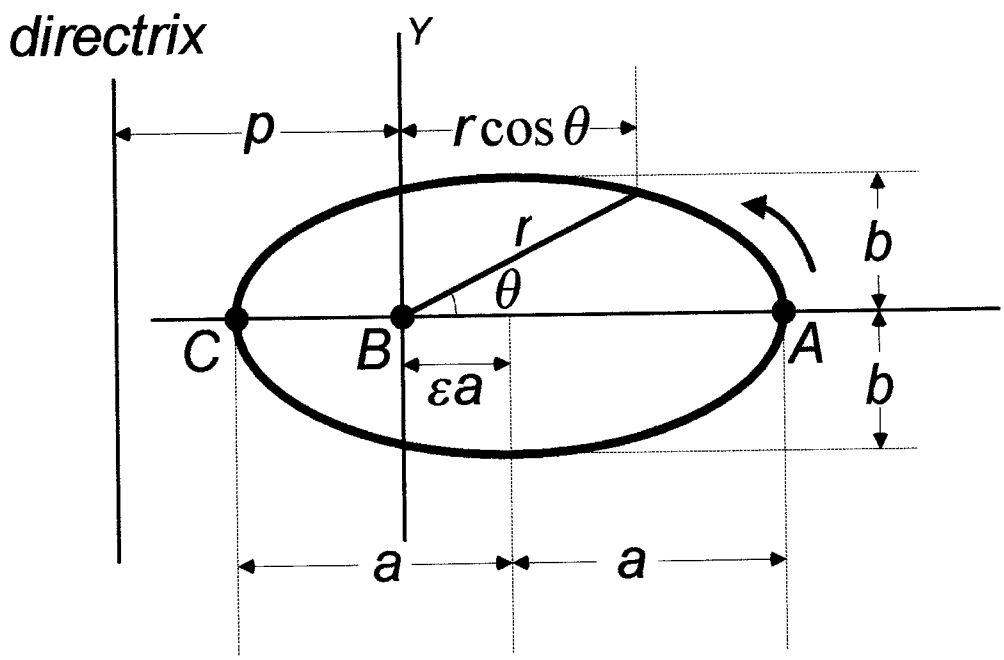

Fig. 2

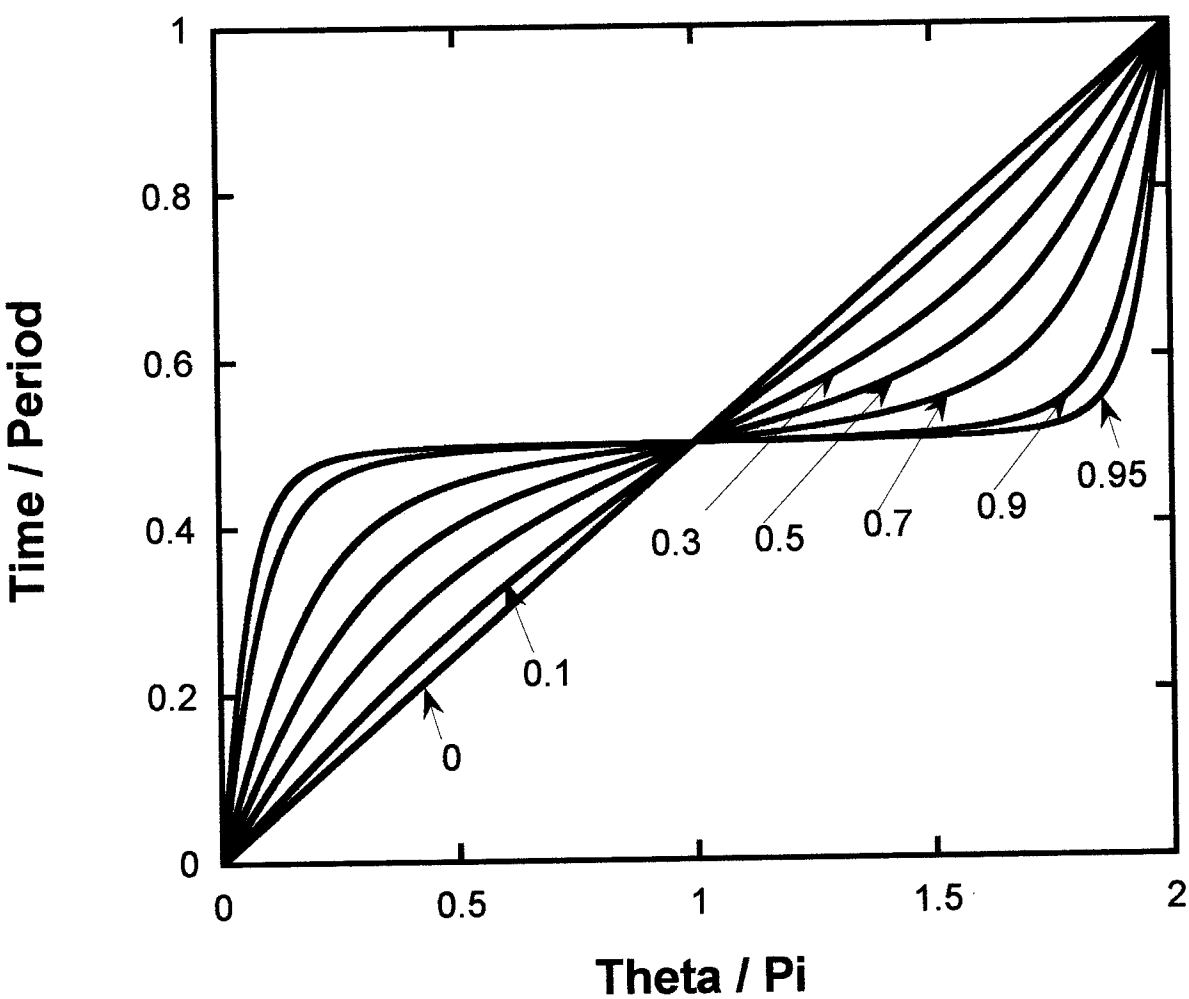

Fig. 3

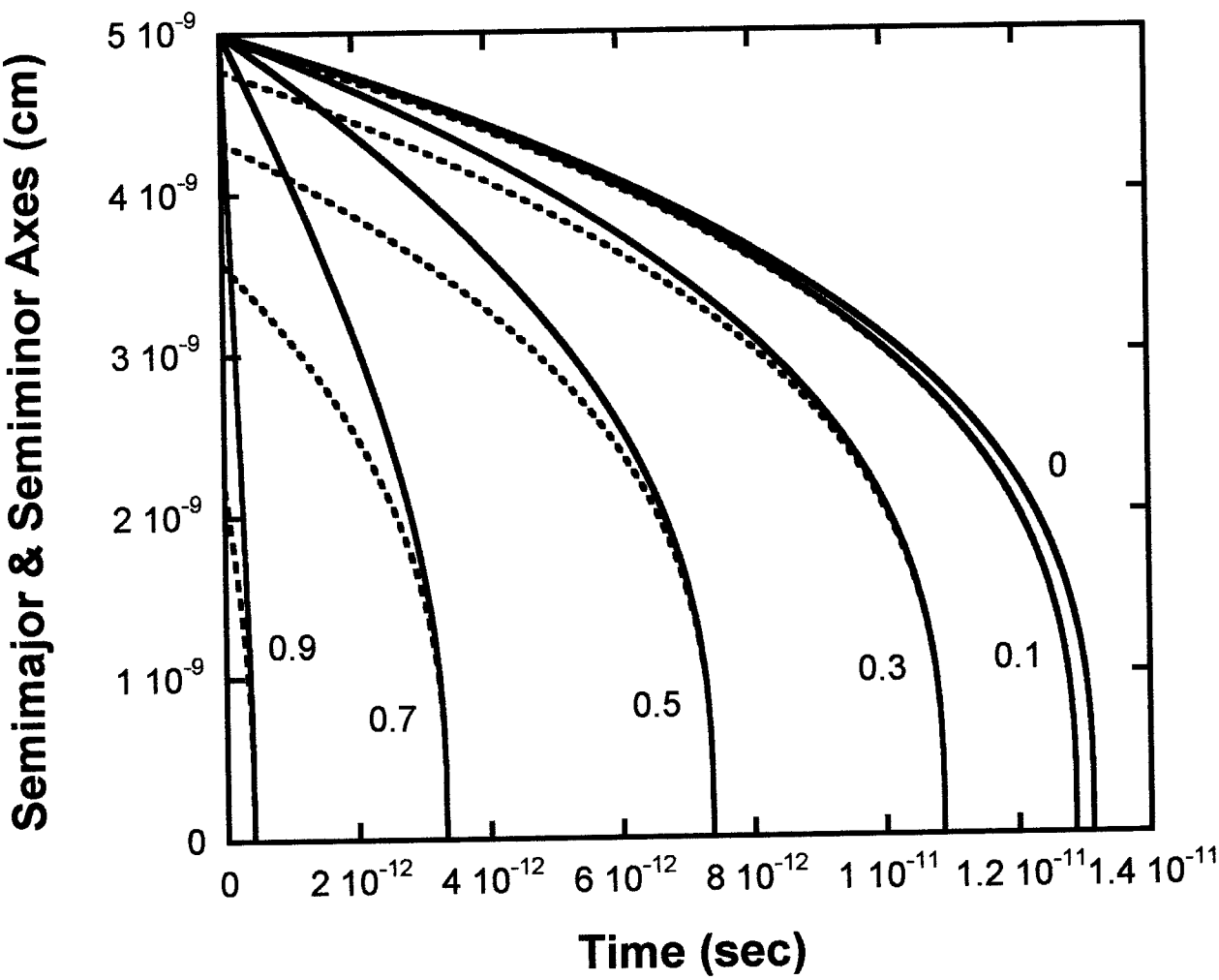
Semimajor & Semiminor Axes (cm)
5 10-9
4 10-9
3 10-9
2 10-9
1 10-9
0
0
2 10-12
4 10-12
6 10-12
8 10-12
1 10-11
1.2 10-11
1.4 10-11
Time (sec)
0
0.1
0.3
0.5
0.7
0.9

Fig. 4(a)

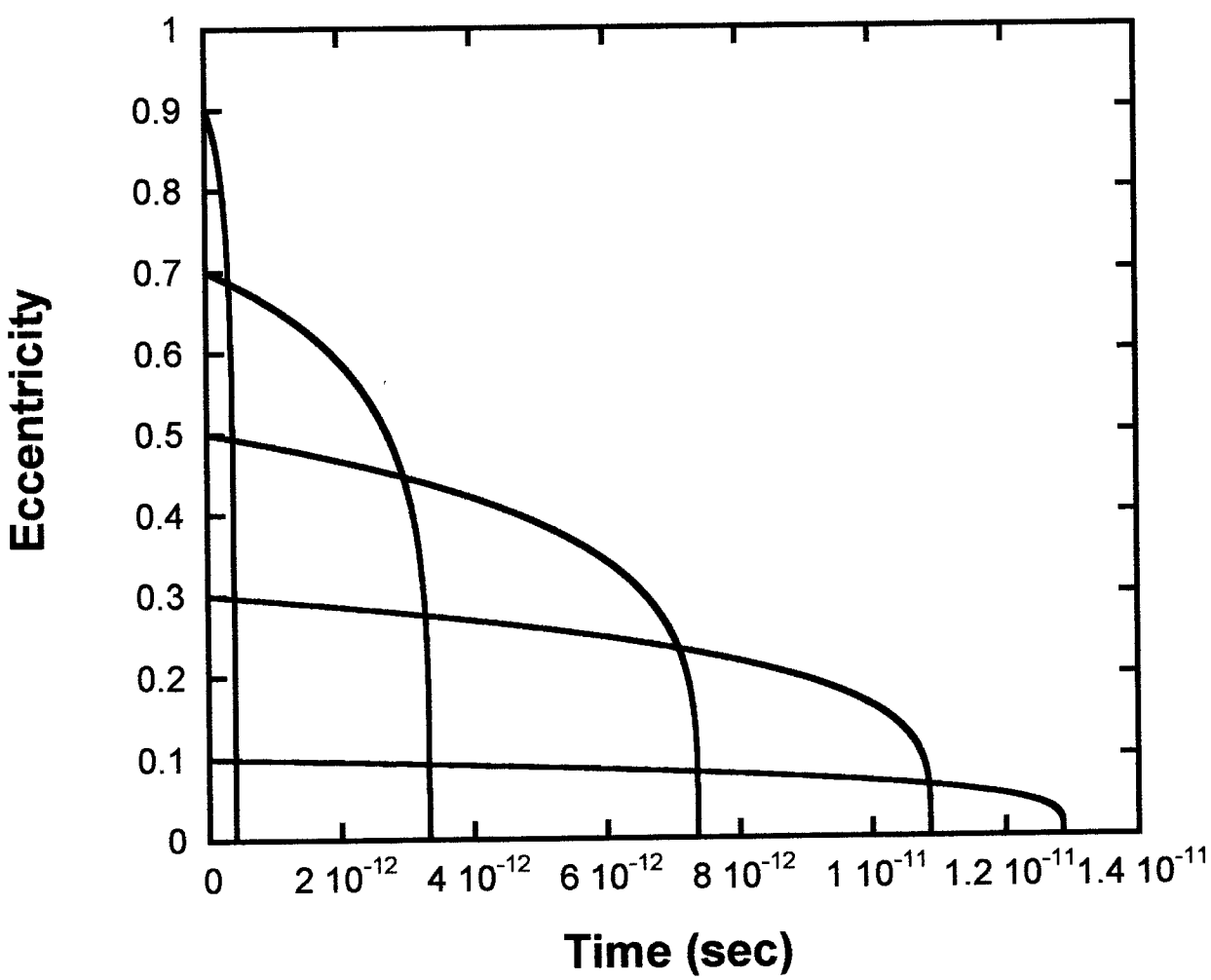
Eccentricity
1
0.9
0.8
0.7
0.6
0.5
0.4
0.3
0.2
0.1
0
0
2 10-12
4 10-12
6 10-12
8 10-12
1 10-11
1.2 10-11
1.4 10-11
Time (sec)

Fig. 4(b)

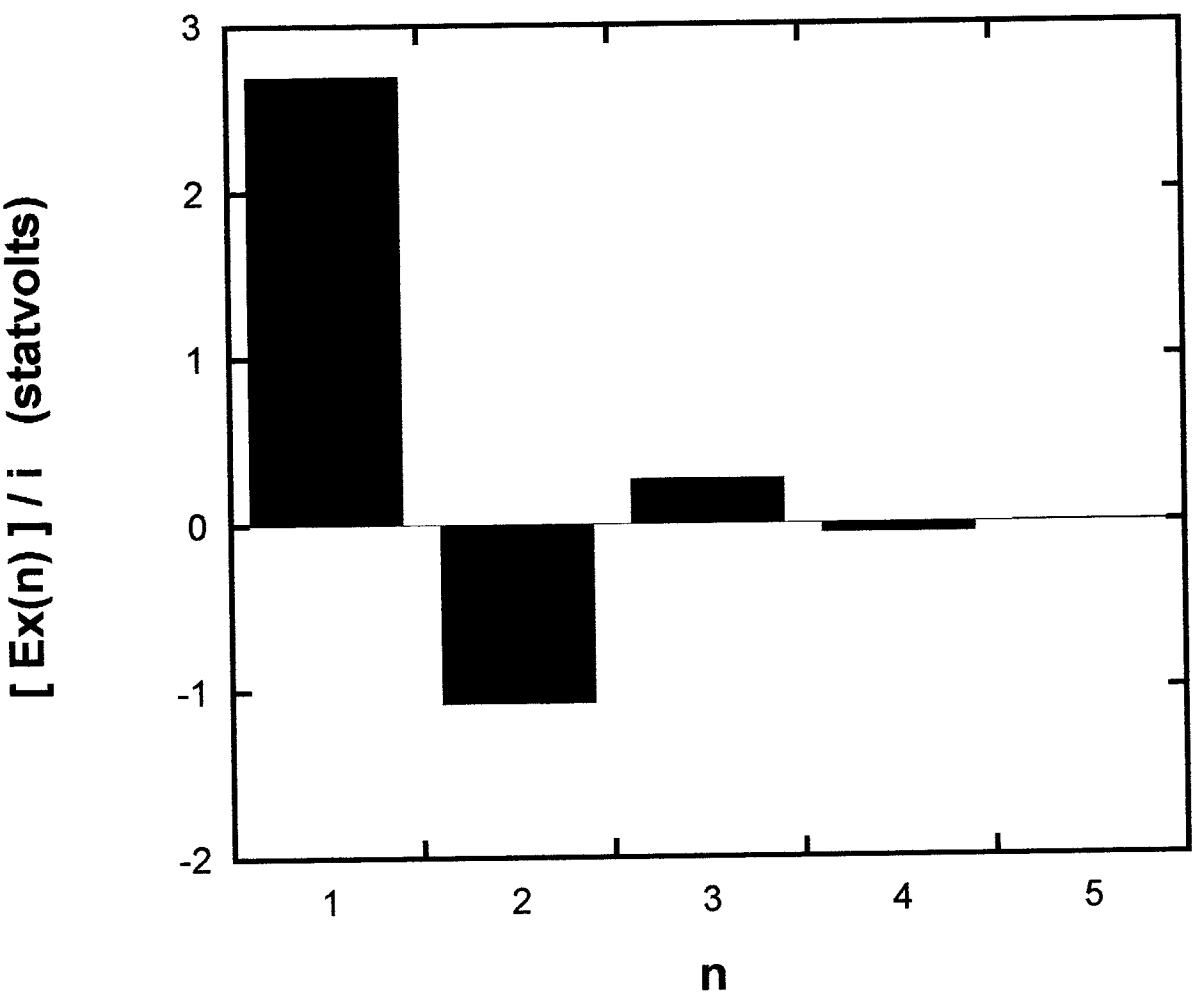

Fig. 5(a)

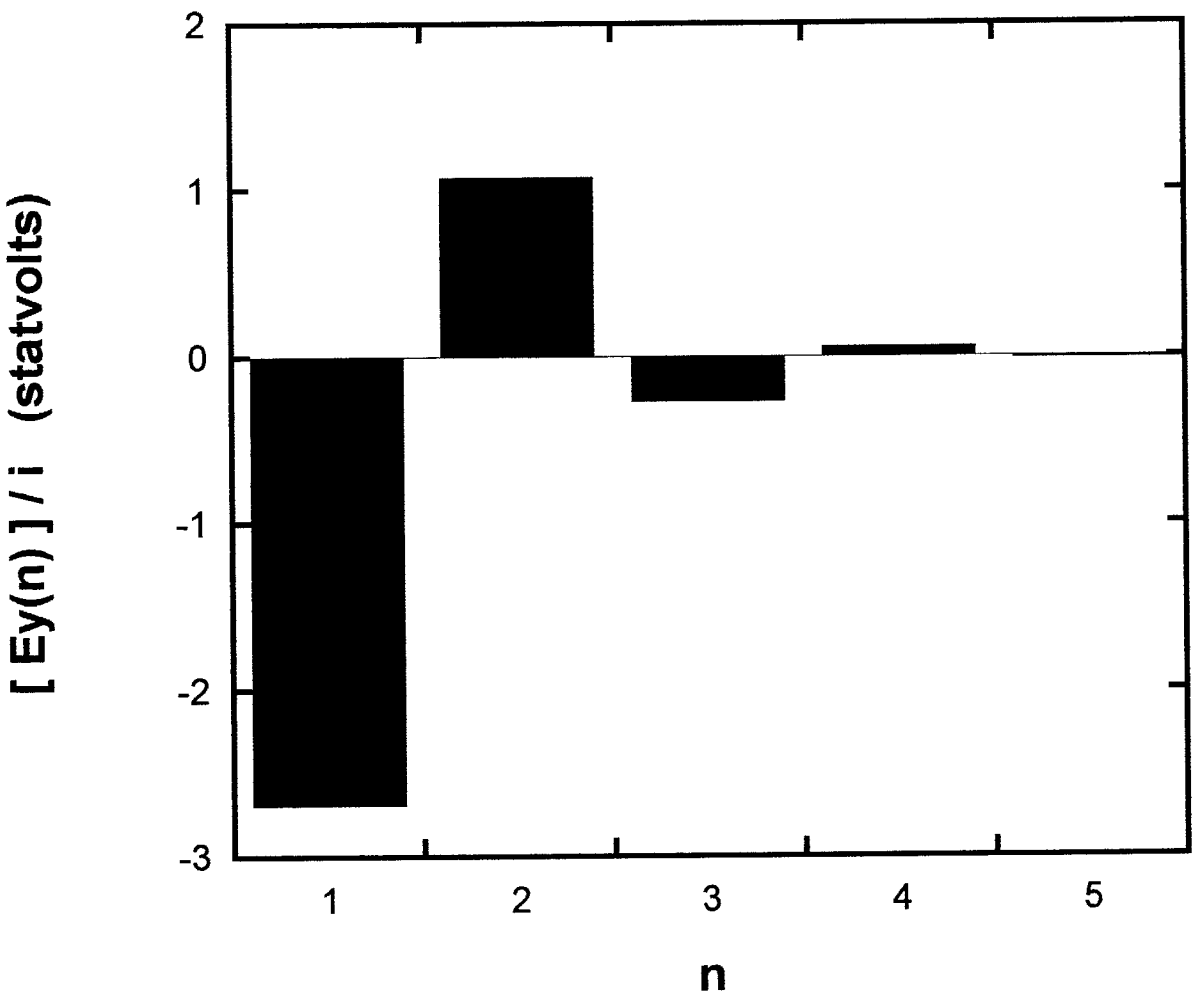

Fig. 5(b)

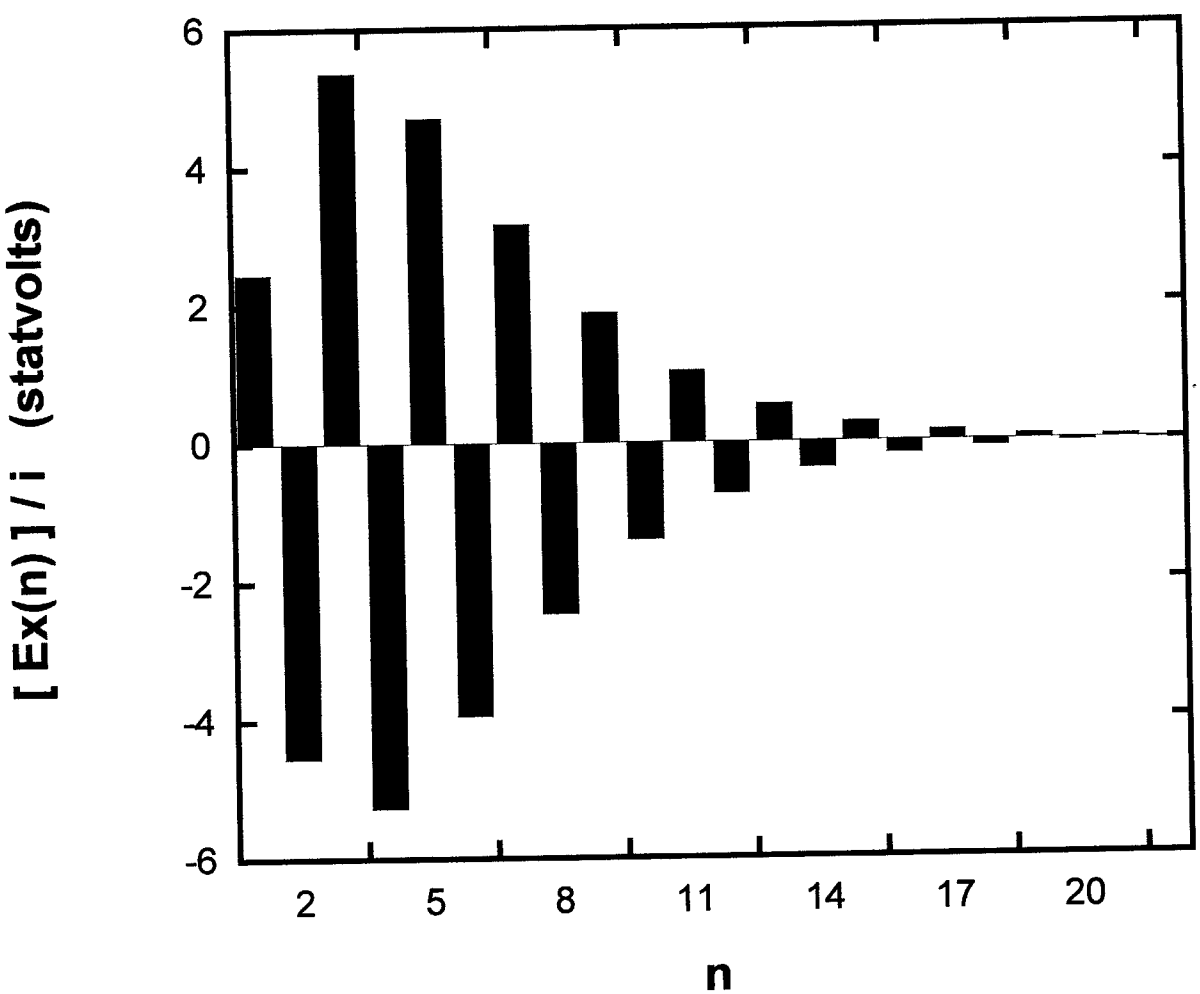

Fig. 5(c)

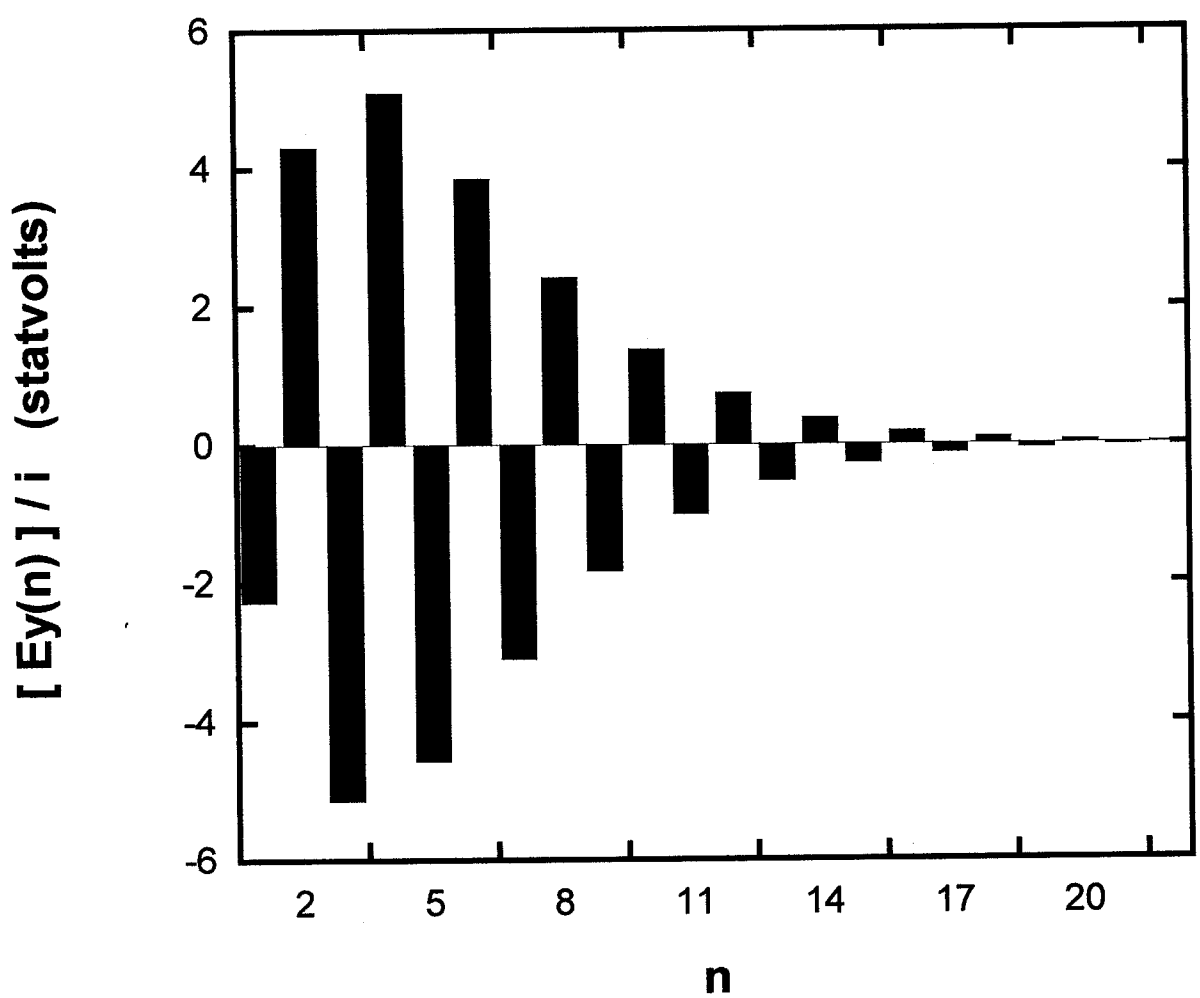

Fig. 5(d)

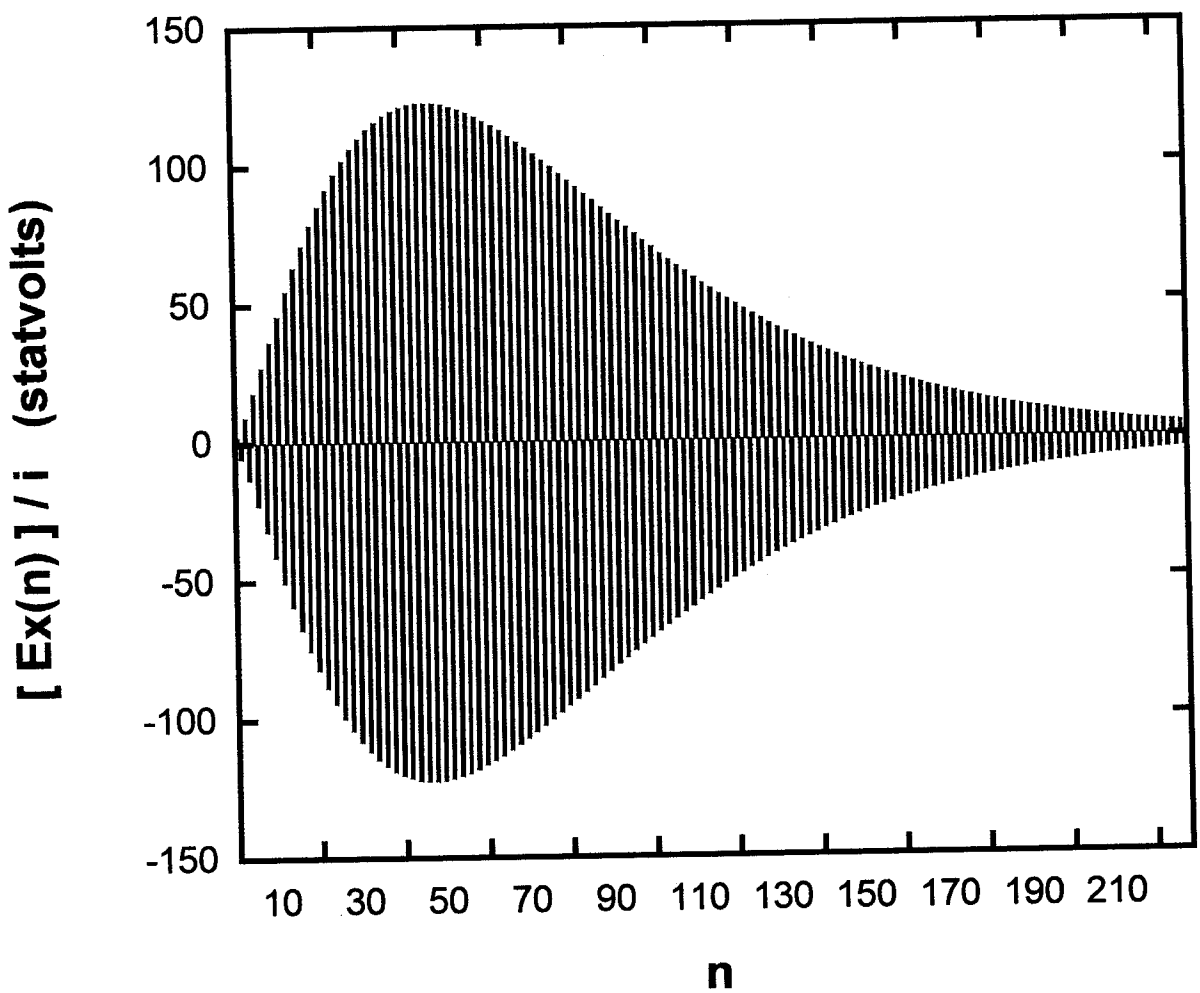
150
100
50
0
-50
-100
-150
10
30
50
70
90
110
130
150
170
190
210
n
[Ex(n)] / i (statvolts)

Fig. 5(e)

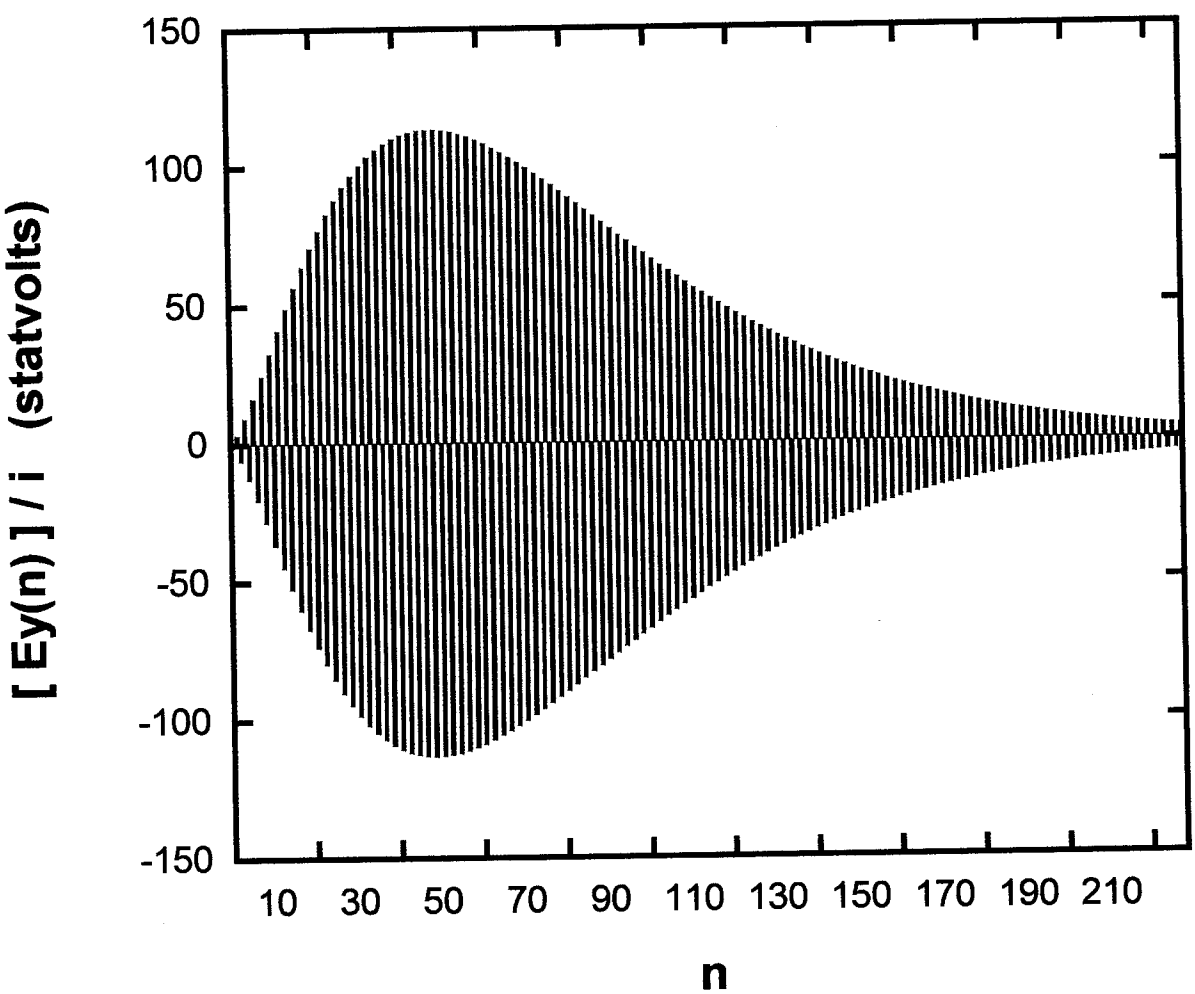
150
100
50
0
-50
-100
-150
10
30
50
70
90
110
130
150
170
190
210
n
[Ey(n)] / i (statvolts)

Fig. 5(f)

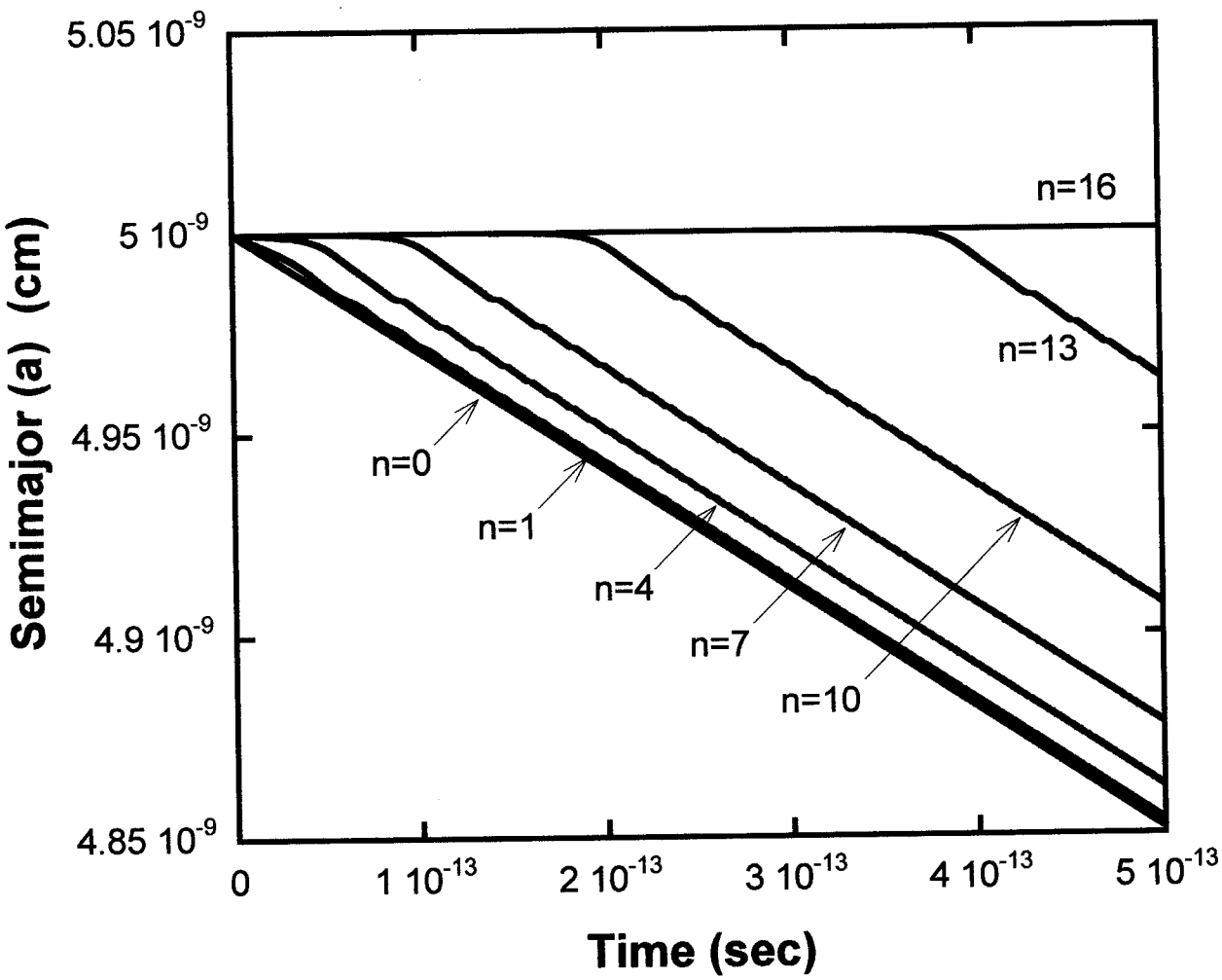
5.05 10-9
5 10-9
4.95 10-9
4.9 10-9
4.85 10-9
Semimajor (a) (cm)
0
1 10-13
2 10-13
3 10-13
4 10-13
5 10-13
Time (sec)
n=16
n=13
n=0
n=1
n=4
n=7
n=10

Fig. 5(g)

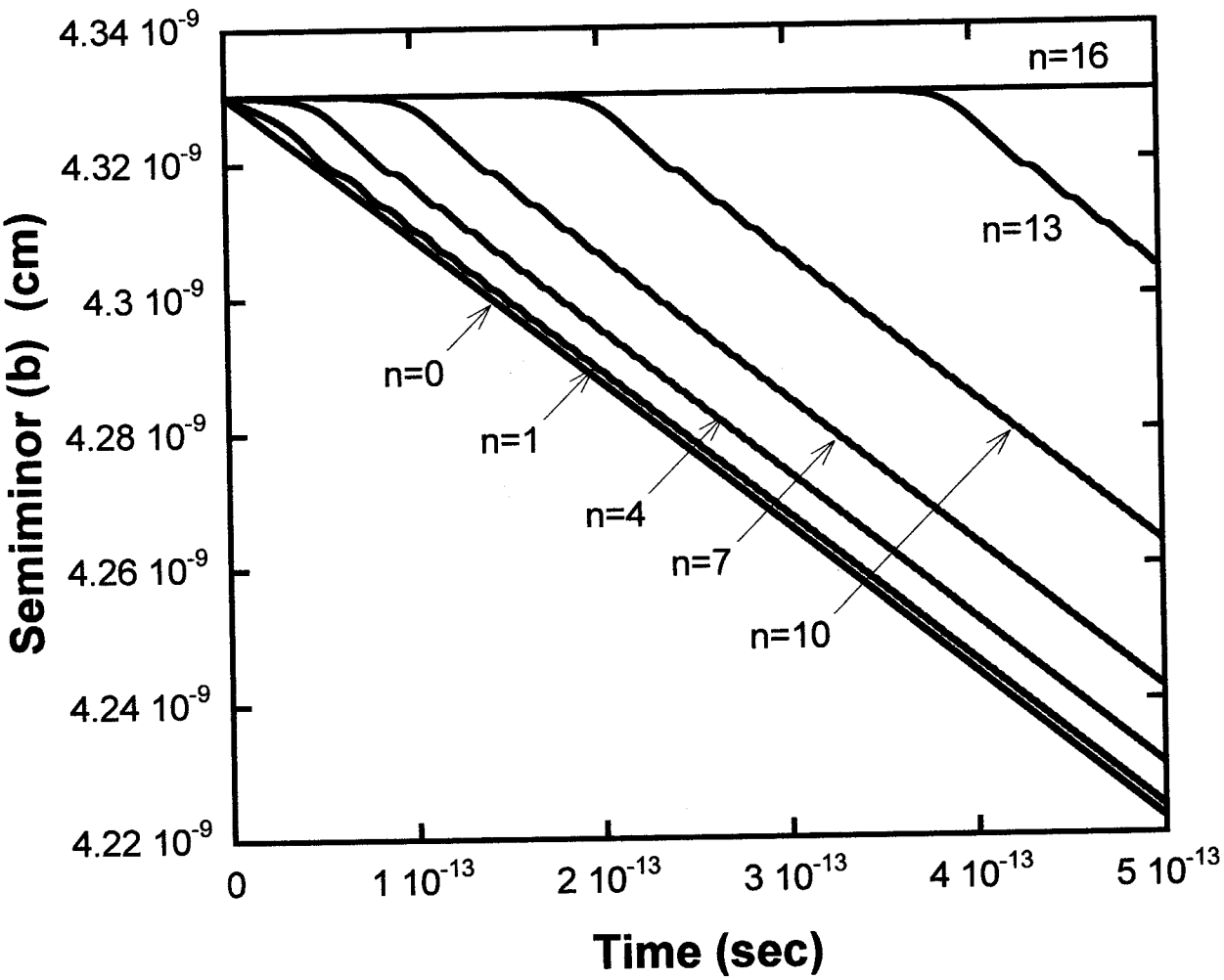
4.34 10-9
4.32 10-9
4.3 10-9
4.28 10-9
4.26 10-9
4.24 10-9
4.22 10-9
Seminor (b) (cm)
0
1 10-13
2 10-13
3 10-13
4 10-13
5 10-13
Time (sec)
n=16
n=13
n=0
n=1
n=4
n=7
n=10

Fig. 5(h)

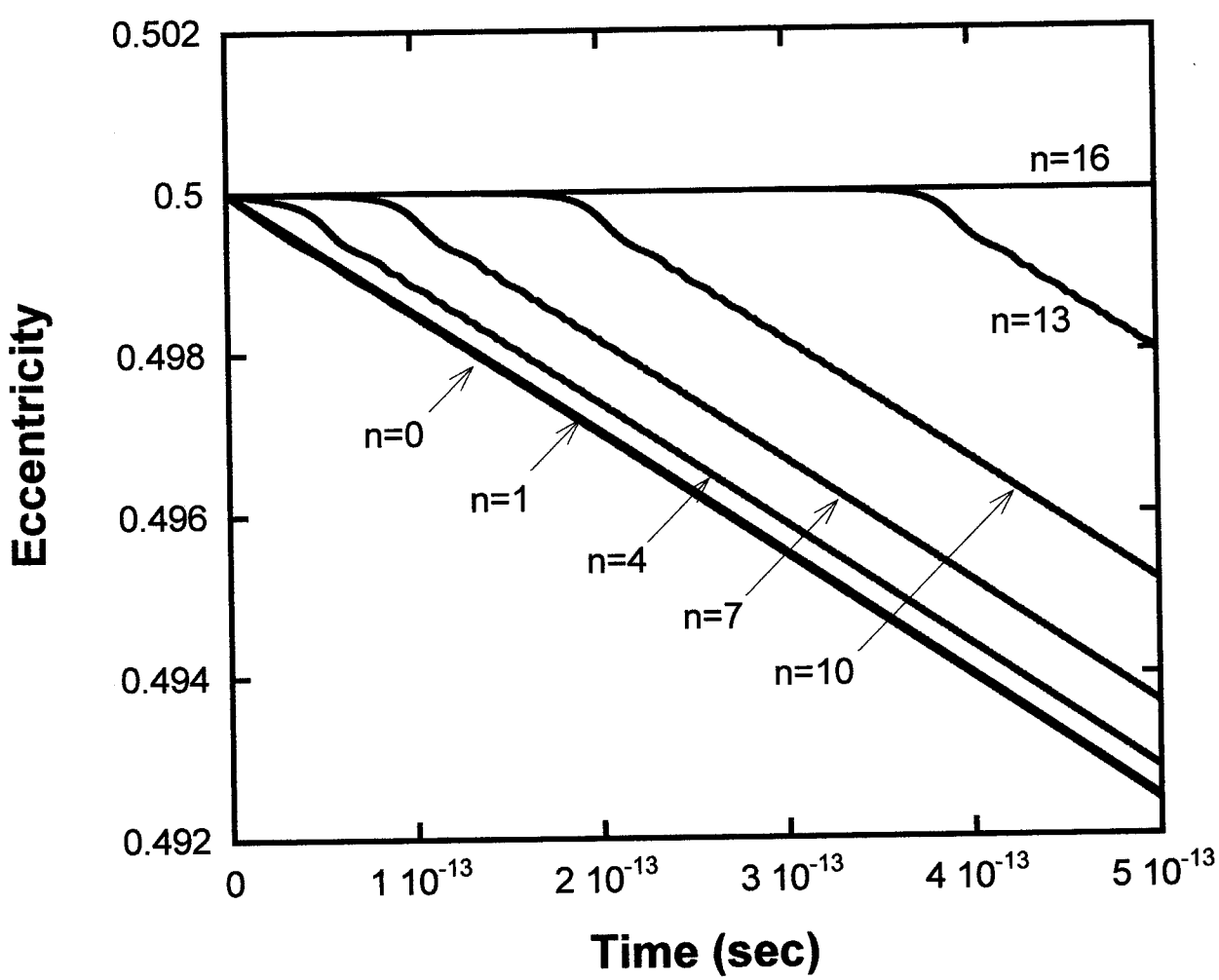
0.502
0.5
0.498
0.496
0.494
0.492
Eccentricity
n=16
n=13
n=0
n=1
n=4
n=7
n=10
0
1 10-13
2 10-13
3 10-13
4 10-13
5 10-13
Time (sec)

Fig. 5(i)

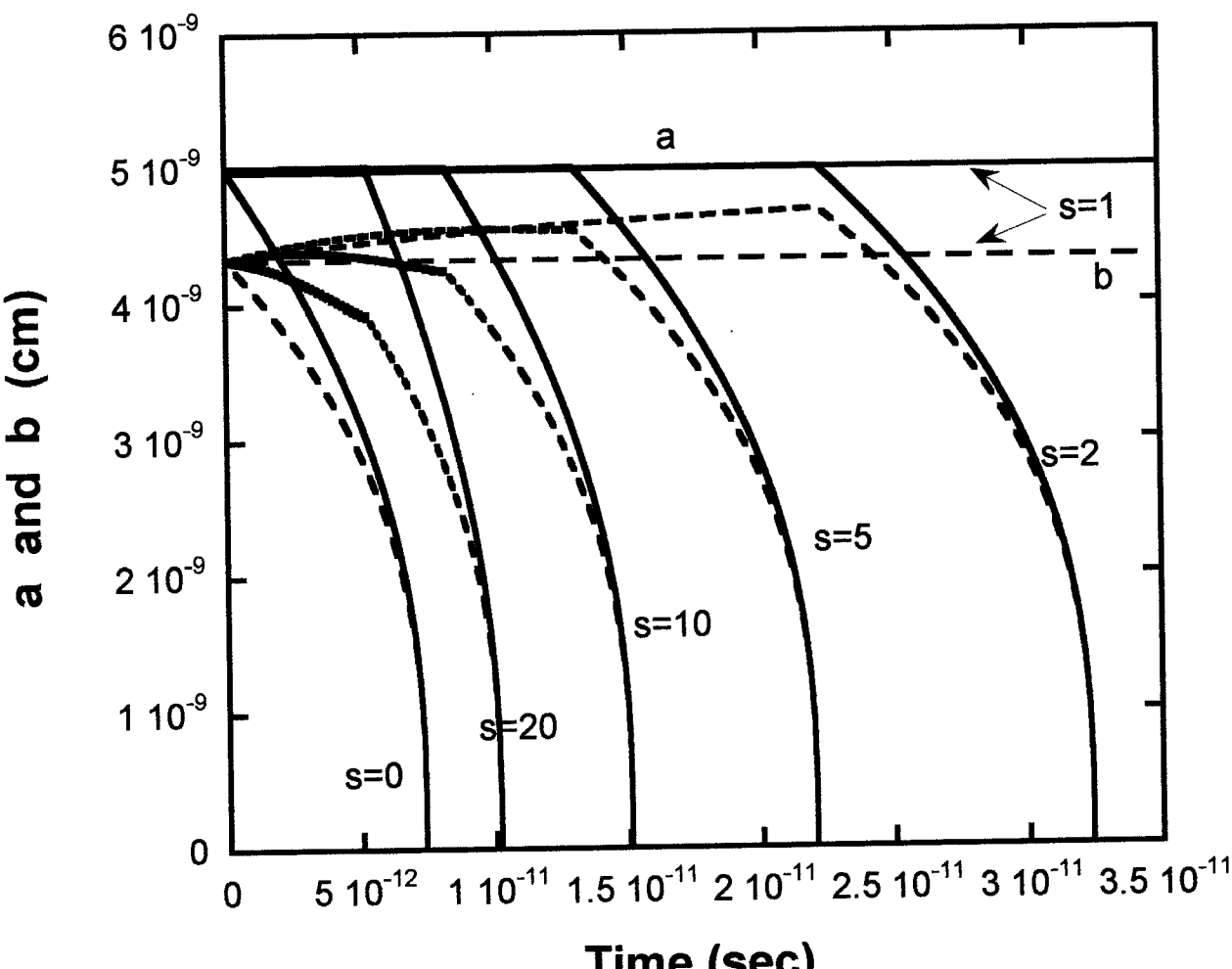
6 10-9
5 10-9
4 10-9
3 10-9
2 10-9
1 10-9
0
a and b (cm)
a
b
s=1
s=2
s=5
s=10
s=20
s=0
0
5 10-12
1 10-11
1.5 10-11
2 10-11
2.5 10-11
3 10-11
3.5 10-11
Time (sec)

Fig. 6(a)

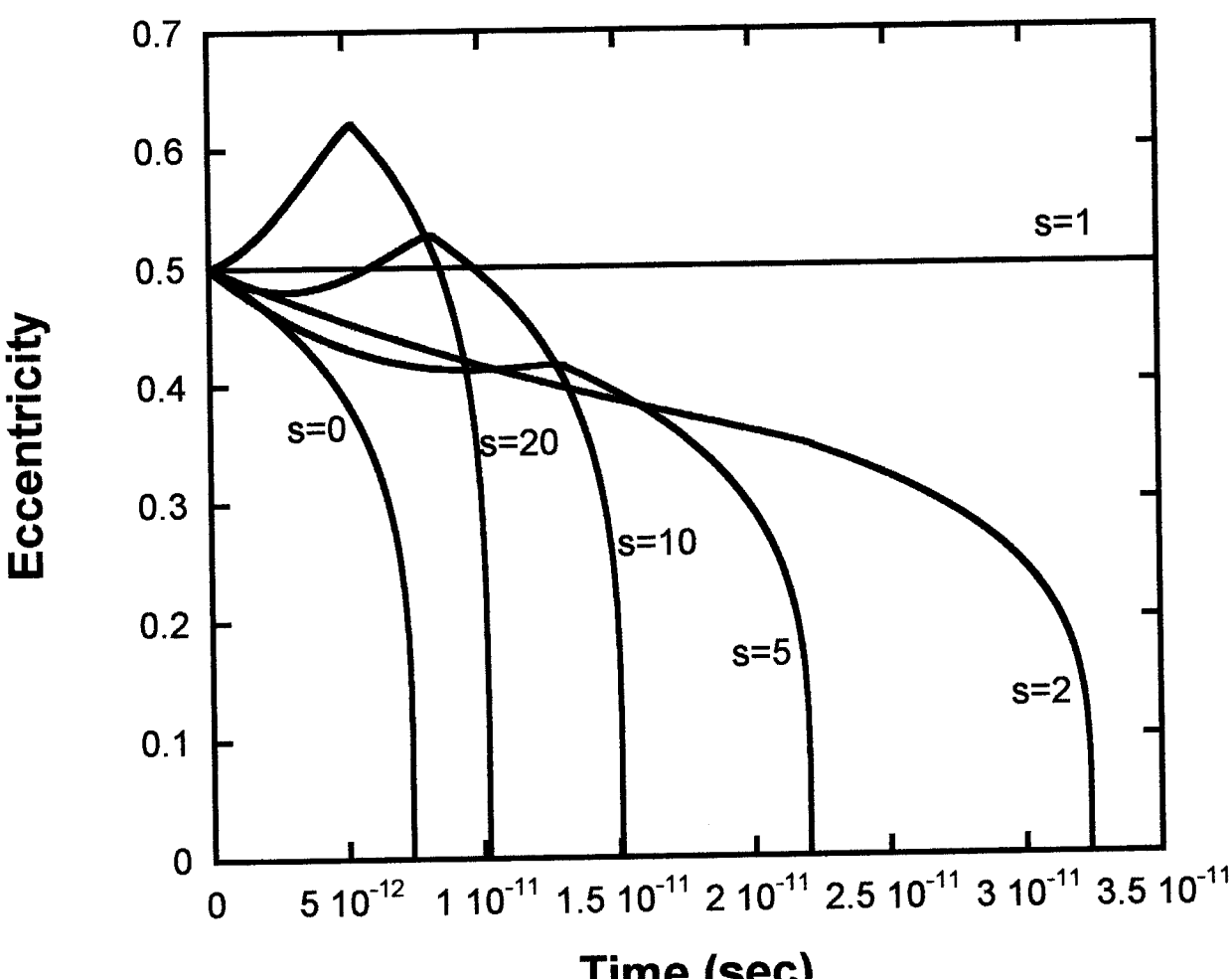
Eccentricity
0.7
0.6
0.5
0.4
0.3
0.2
0.1
0
s=1
s=0
s=20
s=10
s=5
s=2
0
5 10-12
1 10-11
1.5 10-11
2 10-11
2.5 10-11
3 10-11
3.5 10-11
Time (sec)

Fig. 6(b)

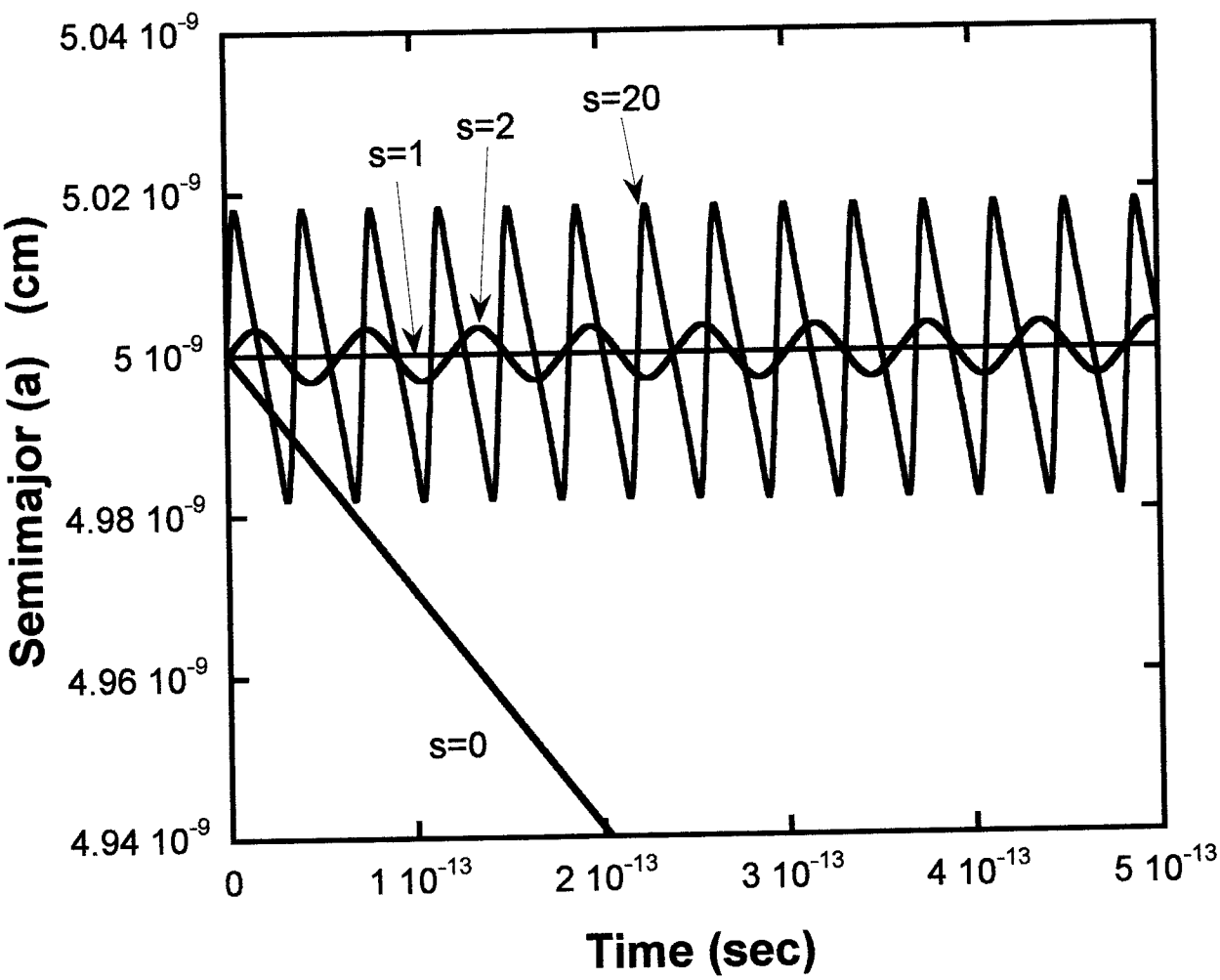
5.04 10-9
5.02 10-9
5 10-9
4.98 10-9
4.96 10-9
4.94 10-9
Semimajor (a) (cm)
s=1
s=2
s=20
s=0
0
1 10-13
2 10-13
3 10-13
4 10-13
5 10-13
Time (sec)

Fig. 6(c)

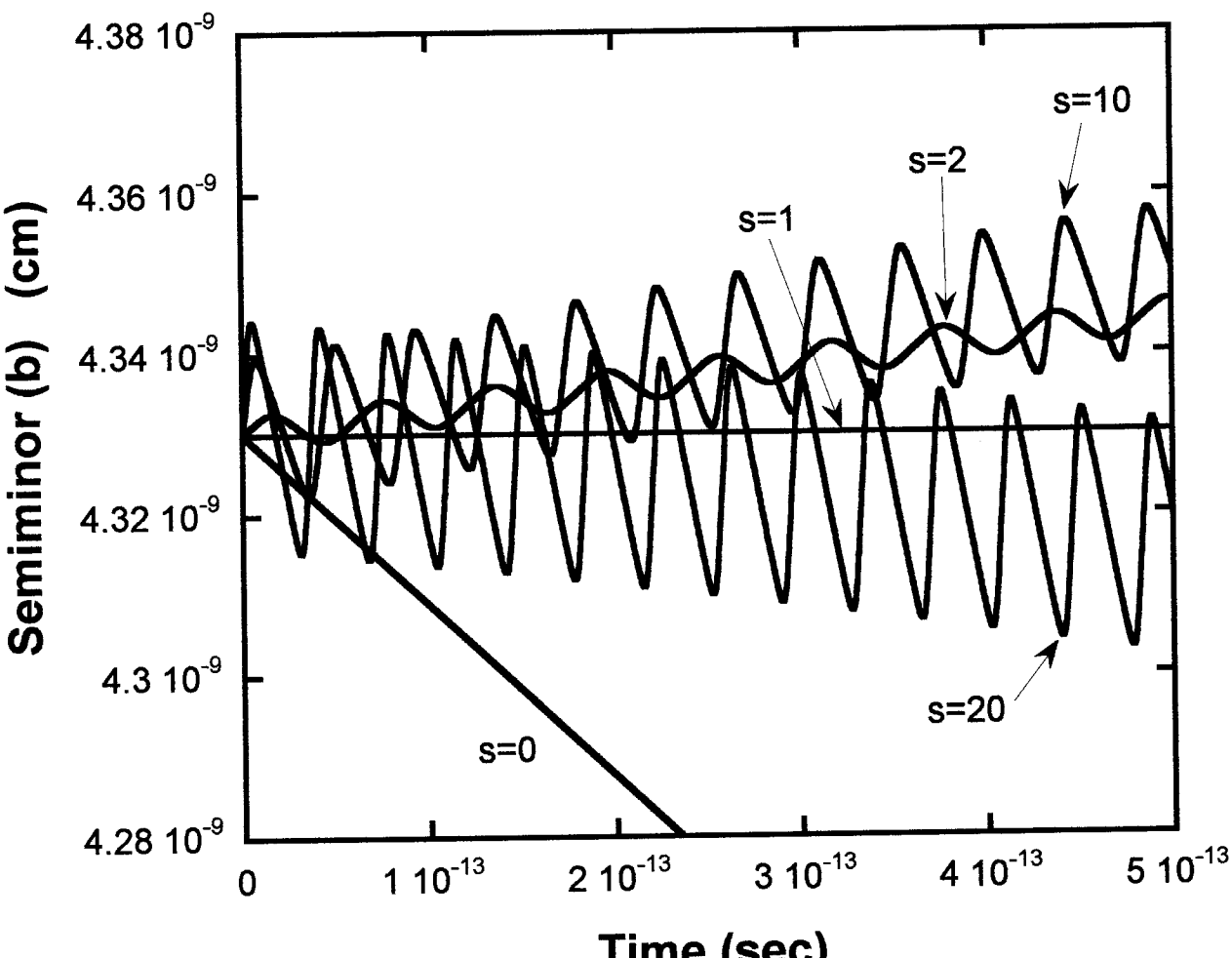
4.38 10-9
4.36 10-9
4.34 10-9
4.32 10-9
4.3 10-9
4.28 10-9
Seminor (b) (cm)
0
1 10-13
2 10-13
3 10-13
4 10-13
5 10-13
Time (sec)
s=0
s=1
s=2
s=10
s=20

Fig. 6(d)

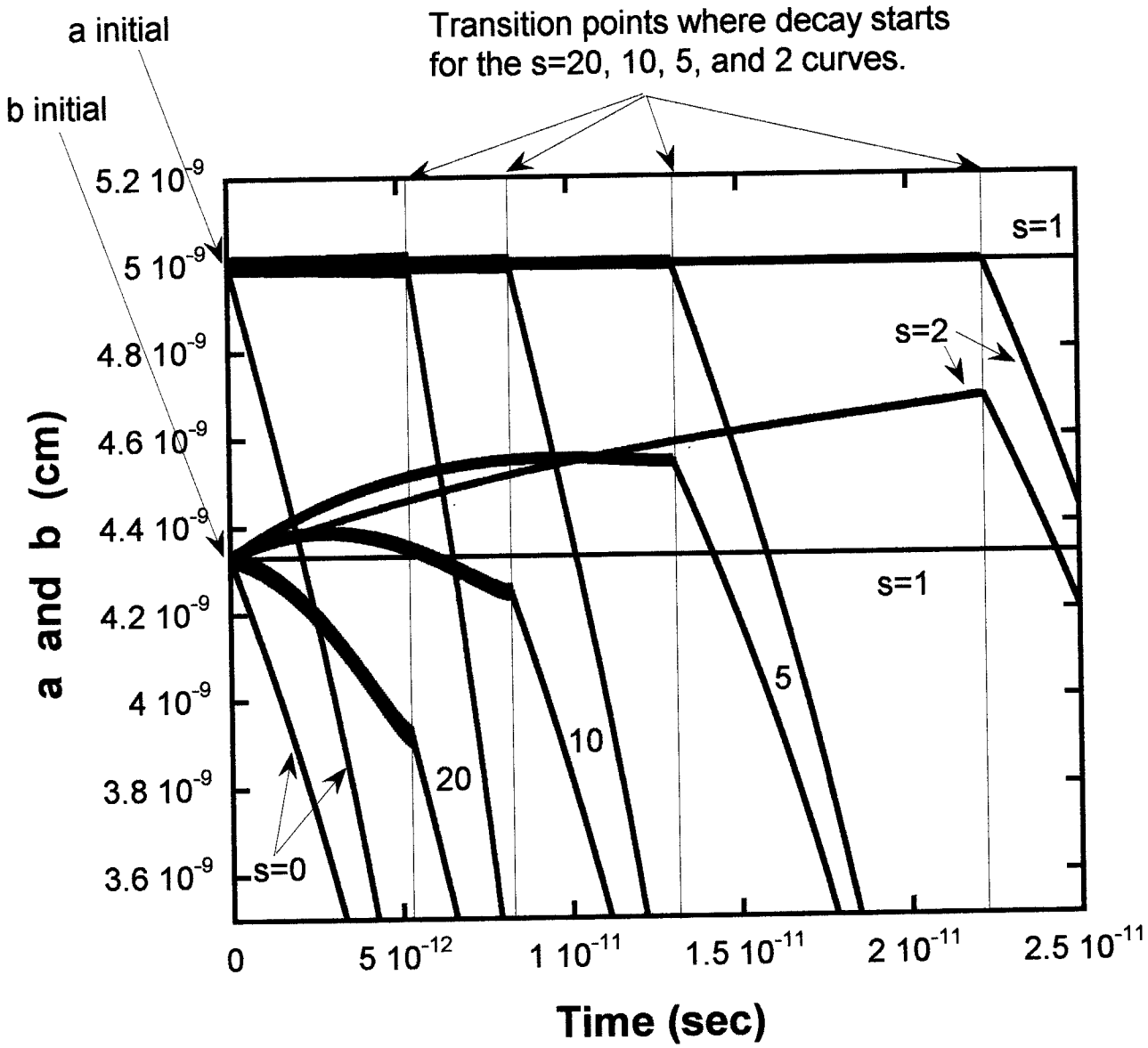
a initial
b initial
Transition points where decay starts
for the s=20, 10, 5, and 2 curves.
5.2 10-9
5 10-9
4.8 10-9
4.6 10-9
4.4 10-9
4.2 10-9
4 10-9
3.8 10-9
3.6 10-9
a and b (cm)
s=1
s=2
s=1
5
10
20
s=0
0
5 10-12
1 10-11
1.5 10-11
2 10-11
2.5 10-11
Time (sec)

Fig. 7(a)

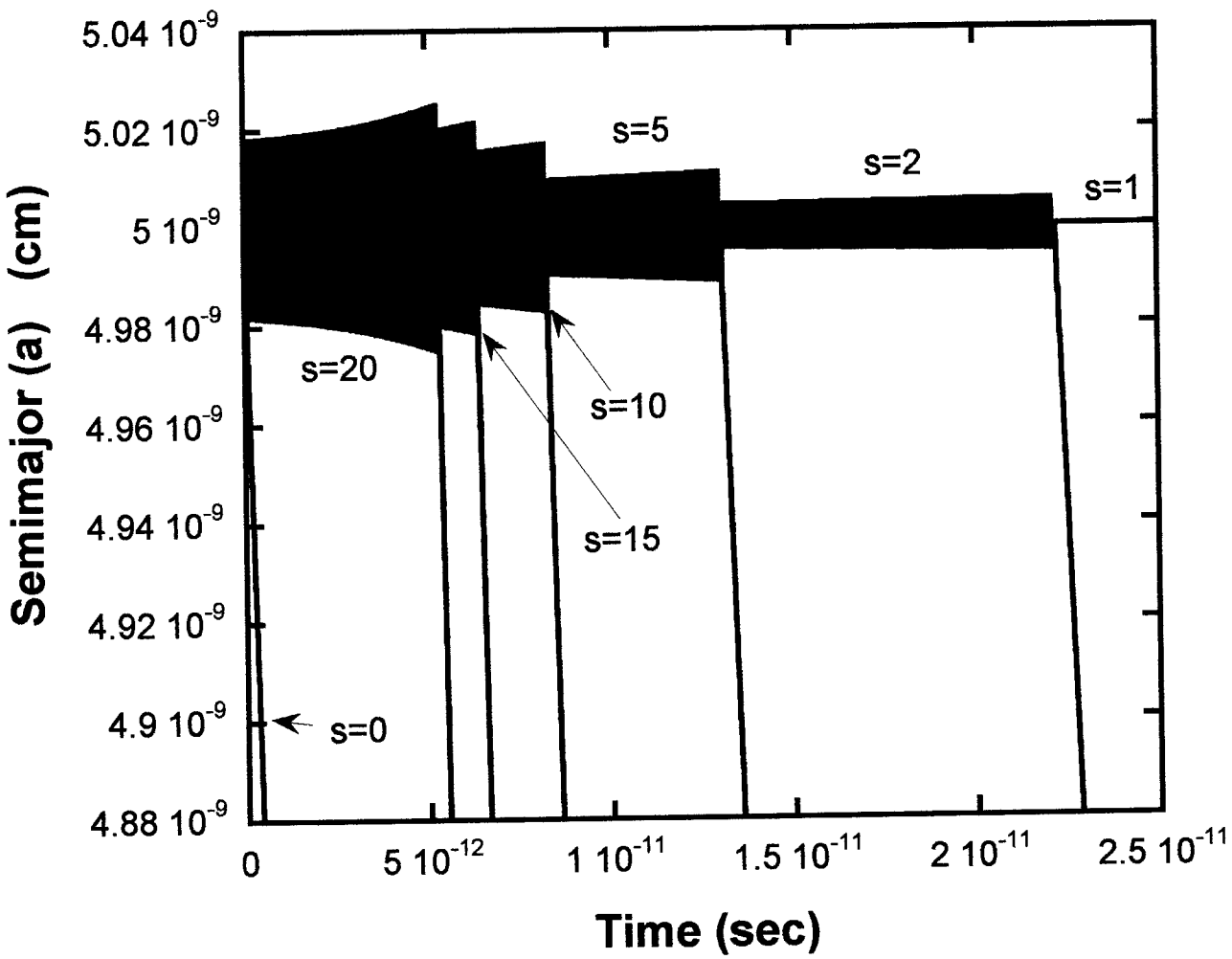
5.04 10-9
5.02 10-9
5 10-9
4.98 10-9
4.96 10-9
4.94 10-9
4.92 10-9
4.9 10-9
4.88 10-9
Semimajor (a) (cm)
s=5
s=2
s=1
s=20
s=10
s=15
s=0
0
5 10-12
1 10-11
1.5 10-11
2 10-11
2.5 10-11
Time (sec)

Fig. 7(b)

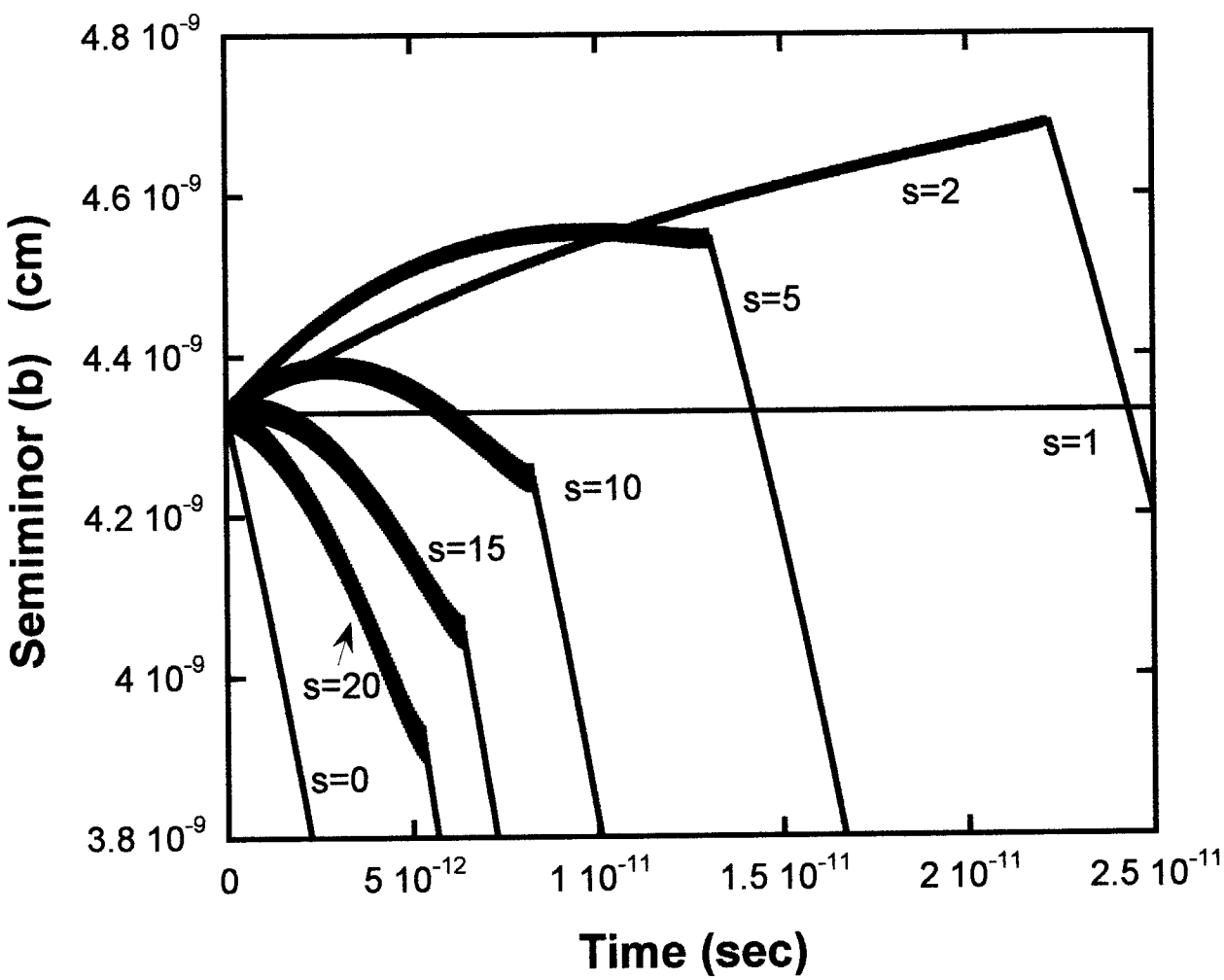
4.8 10-9
4.6 10-9
4.4 10-9
4.2 10-9
4 10-9
3.8 10-9
Seminor (b) (cm)
0
5 10-12
1 10-11
1.5 10-11
2 10-11
2.5 10-11
Time (sec)
s=2
s=5
s=1
s=10
s=15
s=20
s=0

Fig. 7(c)

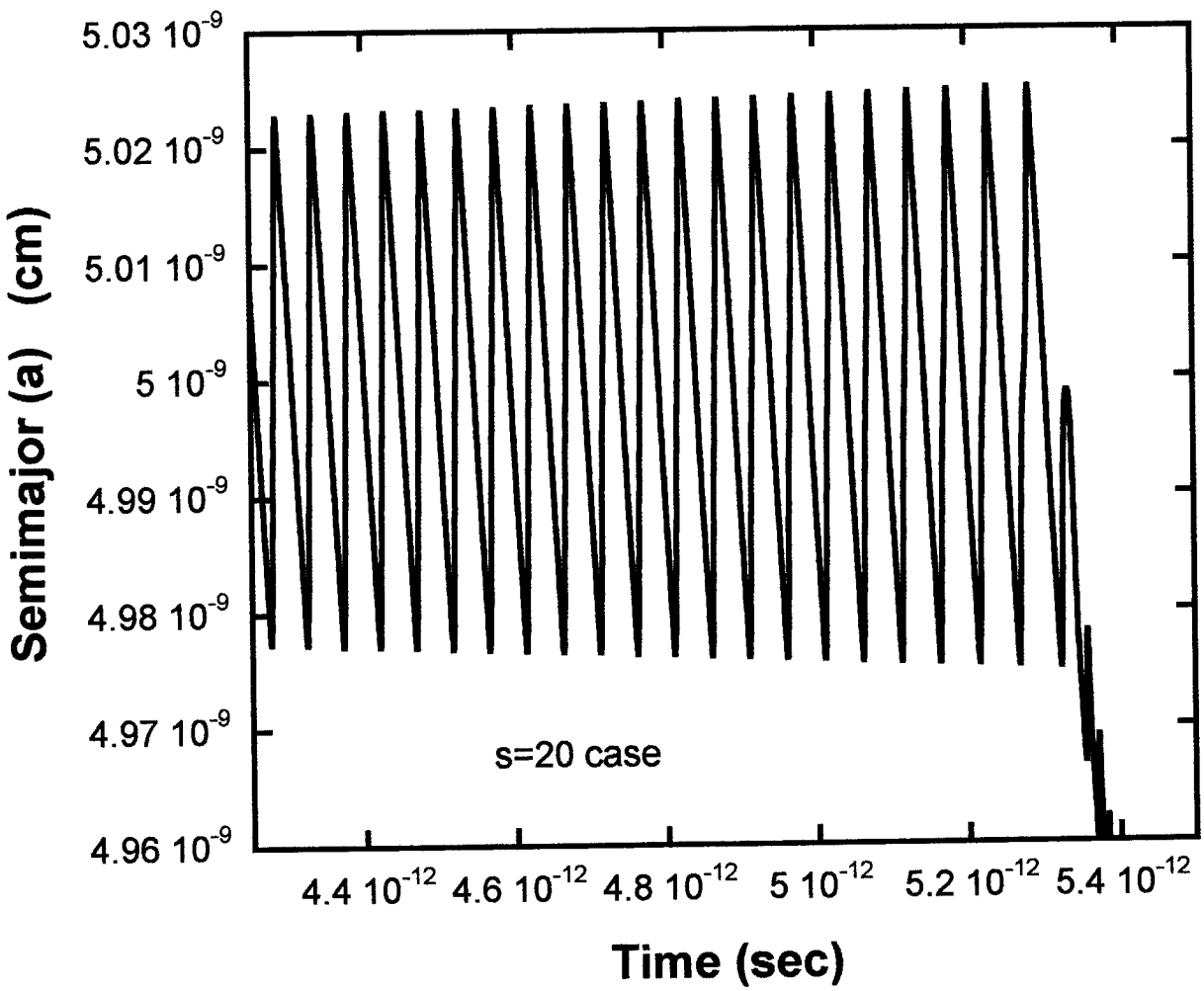
5.03 10^-9
5.02 10^-9
5.01 10^-9
5 10^-9
4.99 10^-9
4.98 10^-9
4.97 10^-9
4.96 10^-9
Semimajor (a) (cm)
s=20 case
4.4 10^-12
4.6 10^-12
4.8 10^-12
5 10^-12
5.2 10^-12
5.4 10^-12
Time (sec)

Fig. 7(d)

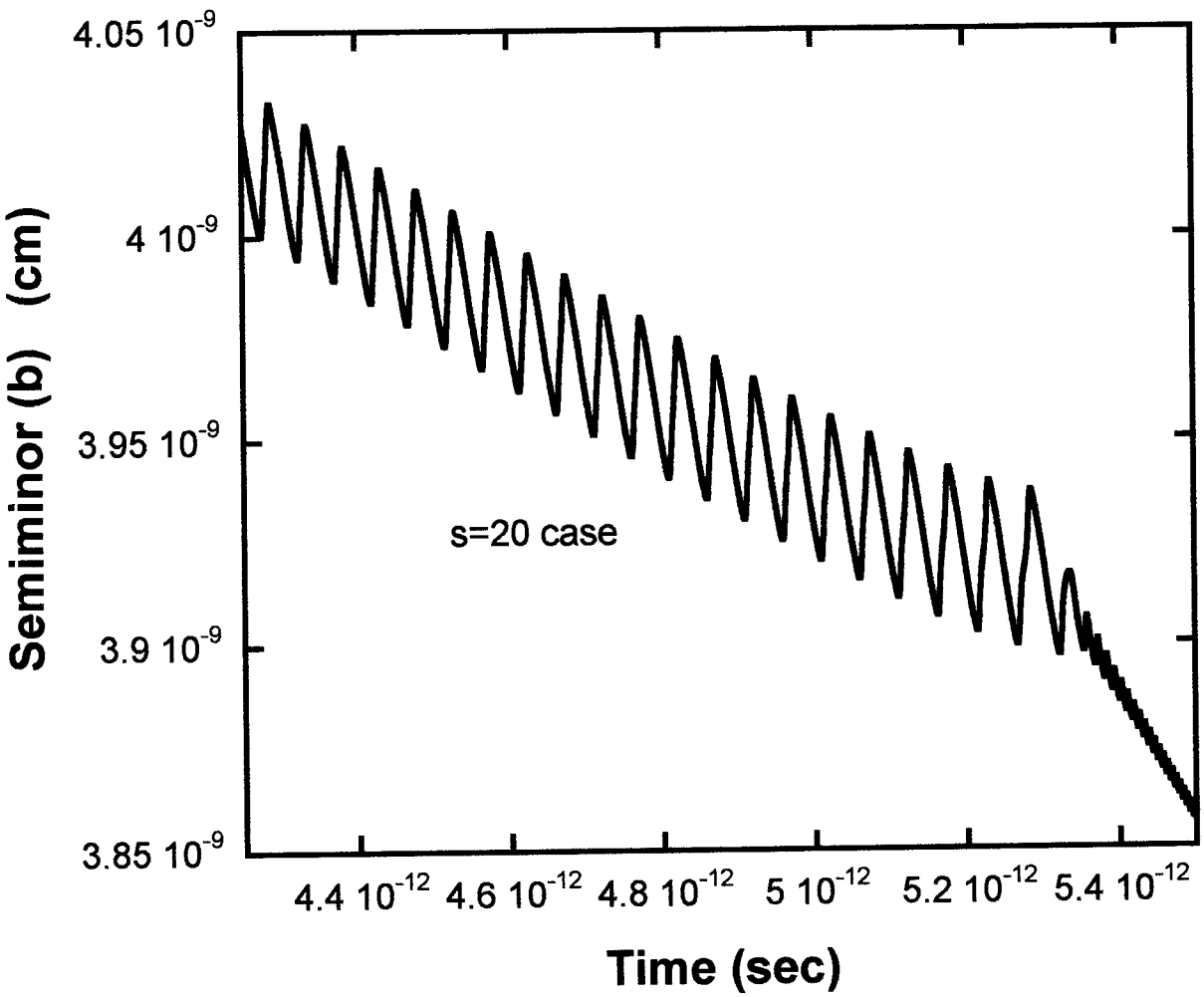
4.05 10-9
4 10-9
3.95 10-9
3.9 10-9
3.85 10-9
Seminor (b) (cm)
s=20 case
4.4 10-12
4.6 10-12
4.8 10-12
5 10-12
5.2 10-12
5.4 10-12
Time (sec)

Fig. 7(e)

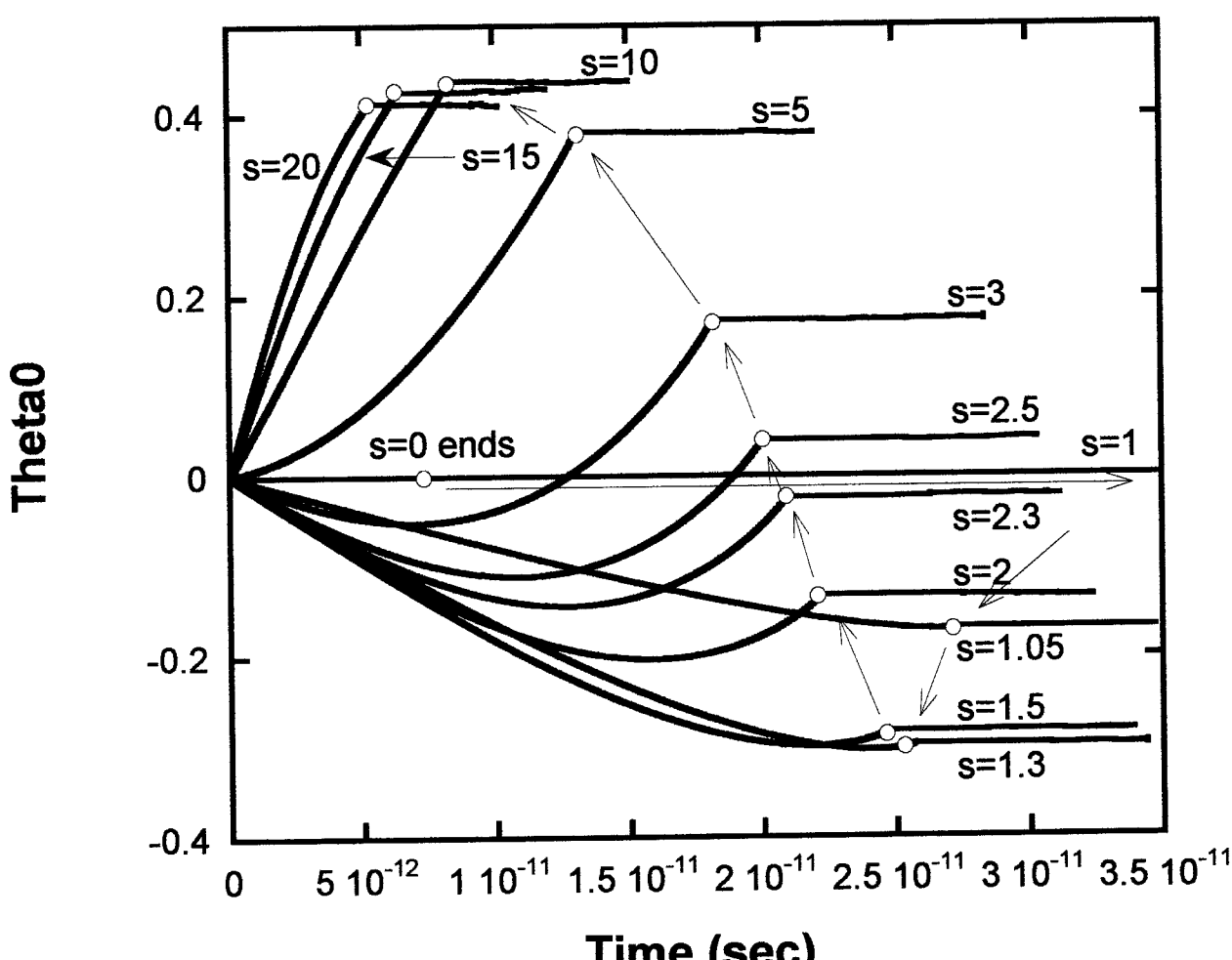
Theta0
0.4
0.2
0
-0.2
-0.4
0
5 10^-12
1 10^-11
1.5 10^-11
2 10^-11
2.5 10^-11
3 10^-11
3.5 10^-11
Time (sec)
s=10
s=5
s=20
s=15
s=3
s=2.5
s=0 ends
s=1
s=2.3
s=2
s=1.05
s=1.5
s=1.3

Fig. 8(a)

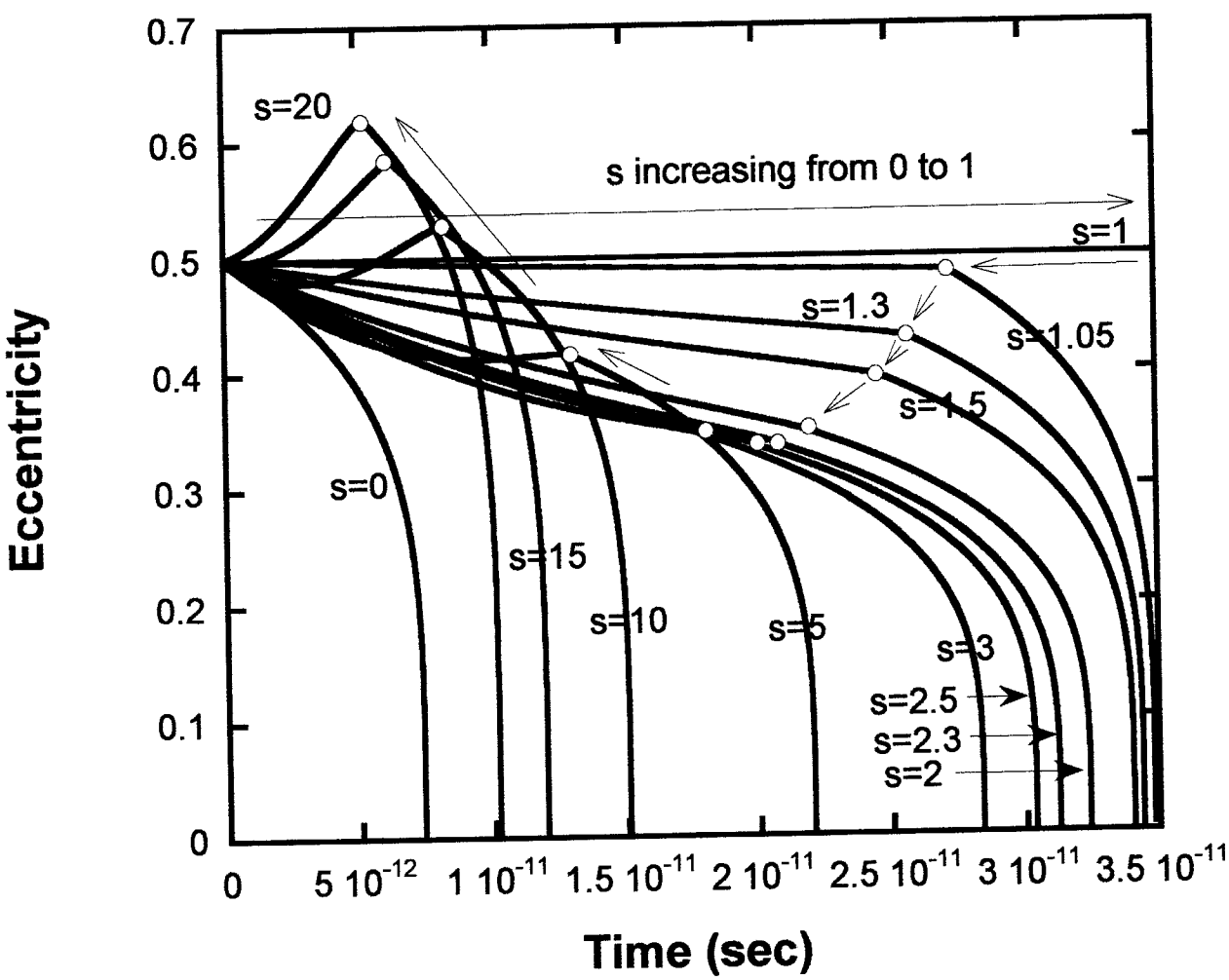
0.7
0.6
0.5
0.4
0.3
0.2
0.1
0
Eccentricity
s=20
s increasing from 0 to 1
s=1
s=1.3
s=1.05
s=1.5
s=0
s=15
s=10
s=5
s=3
s=2.5
s=2.3
s=2
0
5 10-12
1 10-11
1.5 10-11
2 10-11
2.5 10-11
3 10-11
3.5 10-11
Time (sec)

Fig. 8(b)

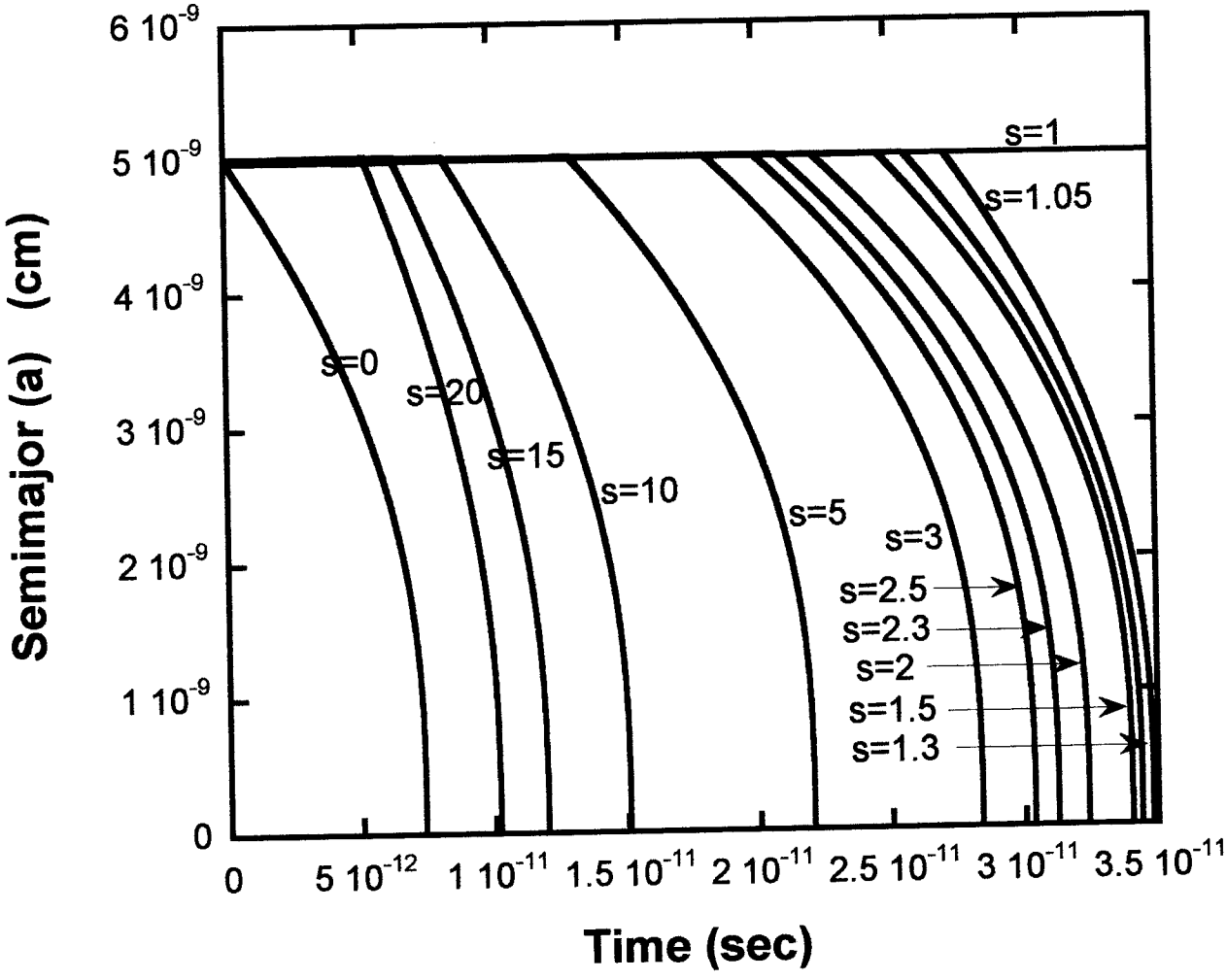
6 10-9
5 10-9
4 10-9
3 10-9
2 10-9
1 10-9
0
Semimajor (a) (cm)
0
5 10-12
1 10-11
1.5 10-11
2 10-11
2.5 10-11
3 10-11
3.5 10-11
Time (sec)
s=1
s=1.05
s=0
s=20
s=15
s=10
s=5
s=3
s=2.5
s=2.3
s=2
s=1.5
s=1.3

Fig. 8(c)

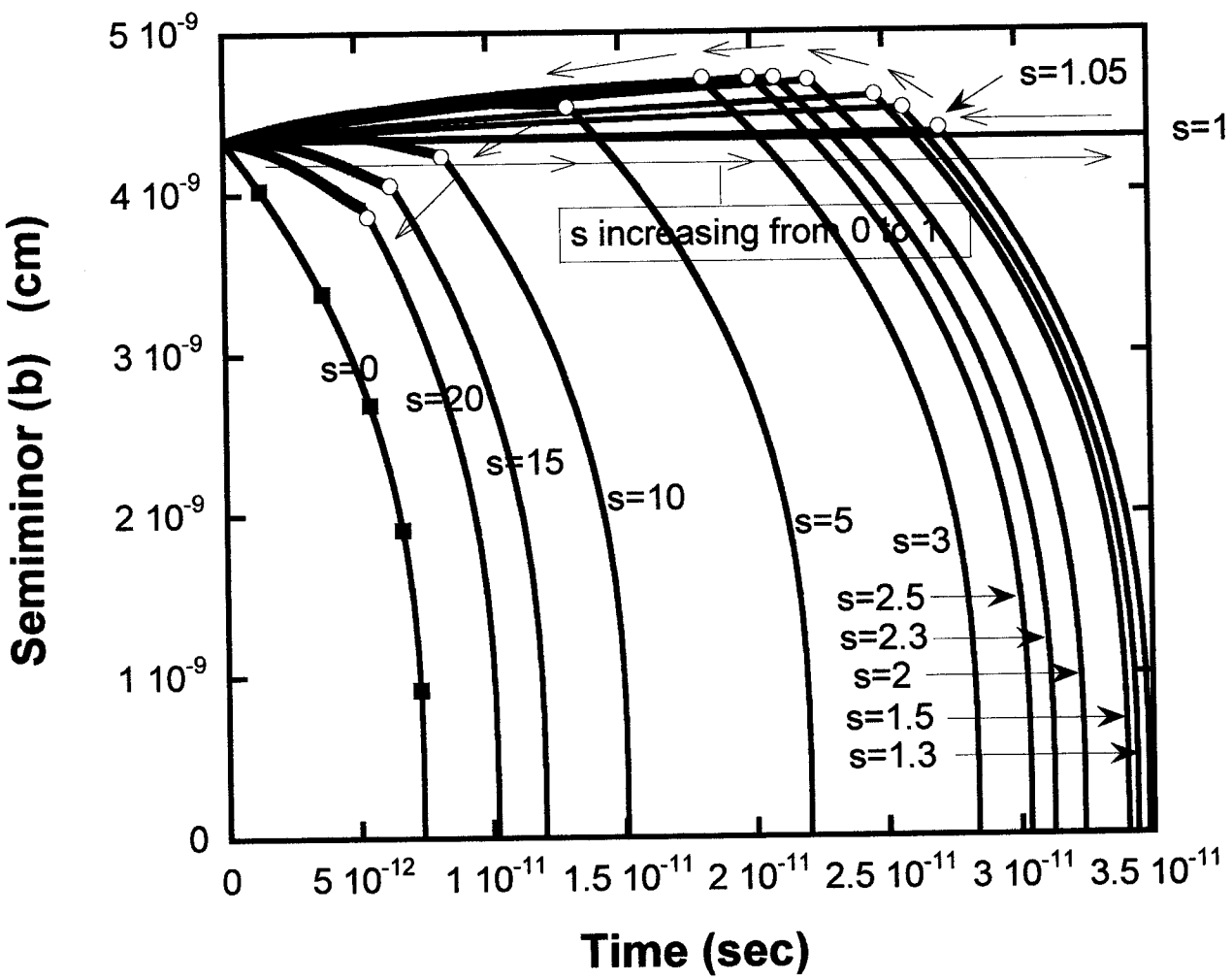
5 10-9
4 10-9
3 10-9
2 10-9
1 10-9
0
Seminor (b) (cm)
0
5 10-12
1 10-11
1.5 10-11
2 10-11
2.5 10-11
3 10-11
3.5 10-11
Time (sec)
s=1.05
s=1
s increasing from 0 to 1
s=0
s=20
s=15
s=10
s=5
s=3
s=2.5
s=2.3
s=2
s=1.5
s=1.3

Fig. 8(d)

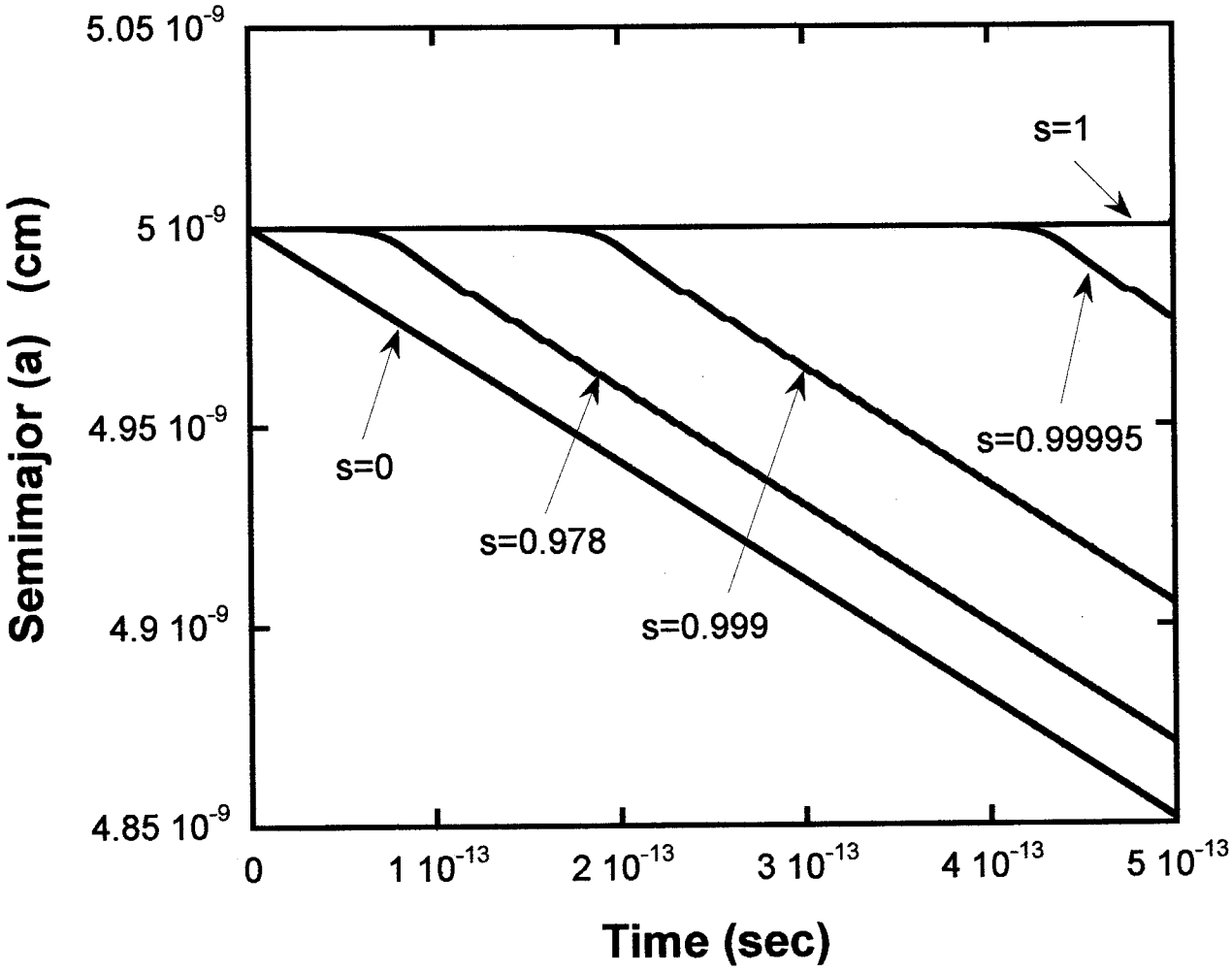
5.05 10-9
5 10-9
4.95 10-9
4.9 10-9
4.85 10-9
Semimajor (a) (cm)
0
1 10-13
2 10-13
3 10-13
4 10-13
5 10-13
Time (sec)
s=1
s=0.99995
s=0
s=0.978
s=0.999

Fig. 9(a)

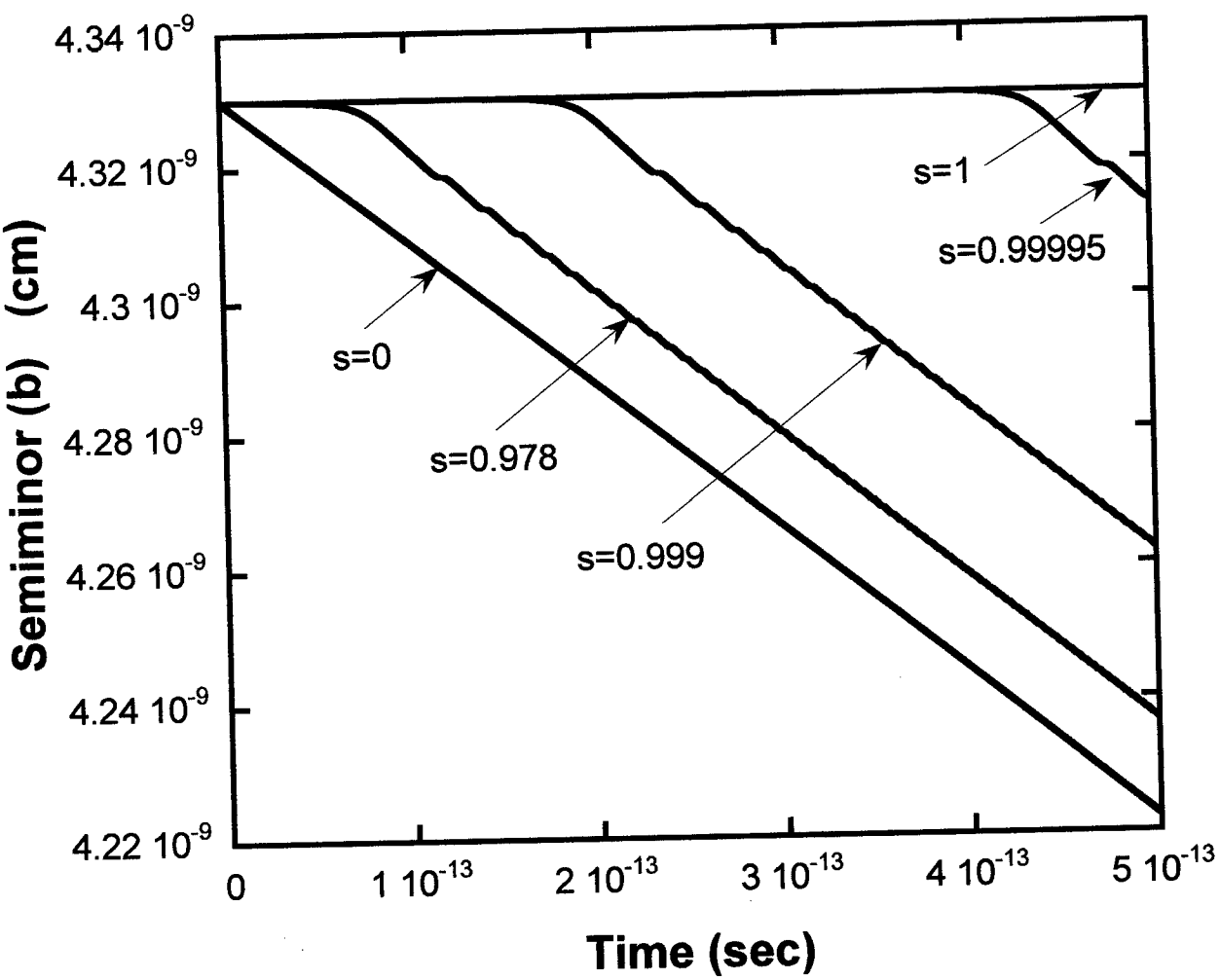
4.34 10-9
4.32 10-9
4.3 10-9
4.28 10-9
4.26 10-9
4.24 10-9
4.22 10-9
Seminor (b) (cm)
0
1 10-13
2 10-13
3 10-13
4 10-13
5 10-13
Time (sec)
s=1
s=0.99995
s=0
s=0.978
s=0.999

Fig. 9(b)

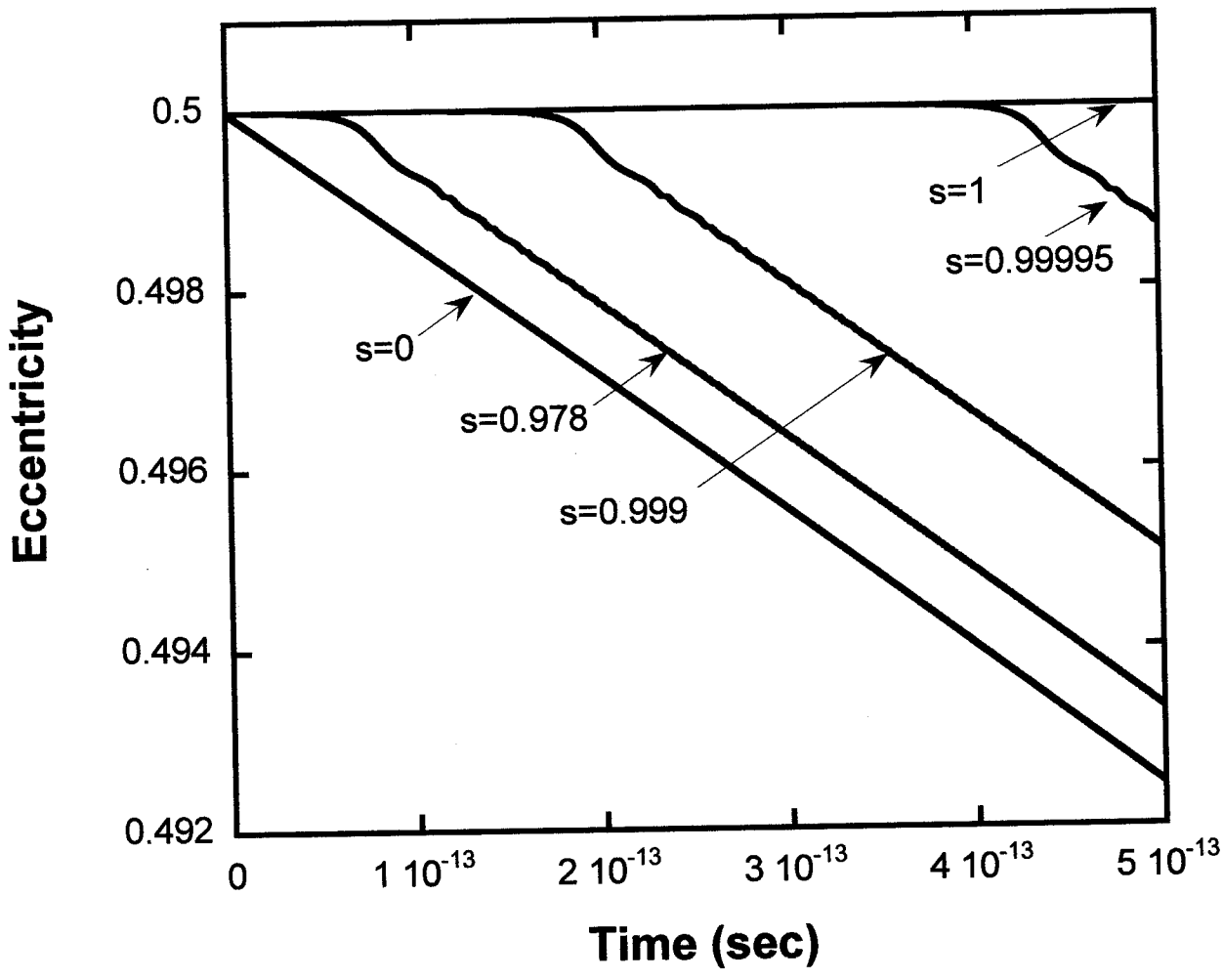
0.5
0.498
0.496
0.494
0.492
Eccentricity
0
1 10-13
2 10-13
3 10-13
4 10-13
5 10-13
Time (sec)
s=1
s=0.99995
s=0
s=0.978
s=0.999

Fig. 9(c)